

ACCEPTED MANUSCRIPT • OPEN ACCESS

Influence of aerosol injection on the liquid chemistry induced by an RF argon plasma jet

To cite this article before publication: Ivana Sremaki *et al* 2021 *Plasma Sources Sci. Technol.* in press <https://doi.org/10.1088/1361-6595/abe176>

Manuscript version: Accepted Manuscript

Accepted Manuscript is “the version of the article accepted for publication including all changes made as a result of the peer review process, and which may also include the addition to the article by IOP Publishing of a header, an article ID, a cover sheet and/or an ‘Accepted Manuscript’ watermark, but excluding any other editing, typesetting or other changes made by IOP Publishing and/or its licensors”

This Accepted Manuscript is © 2021 IOP Publishing Ltd.

As the Version of Record of this article is going to be / has been published on a gold open access basis under a CC BY 3.0 licence, this Accepted Manuscript is available for reuse under a CC BY 3.0 licence immediately.

Everyone is permitted to use all or part of the original content in this article, provided that they adhere to all the terms of the licence <https://creativecommons.org/licenses/by/3.0>

Although reasonable endeavours have been taken to obtain all necessary permissions from third parties to include their copyrighted content within this article, their full citation and copyright line may not be present in this Accepted Manuscript version. Before using any content from this article, please refer to the Version of Record on IOPscience once published for full citation and copyright details, as permissions may be required. All third party content is fully copyright protected and is not published on a gold open access basis under a CC BY licence, unless that is specifically stated in the figure caption in the Version of Record.

View the [article online](#) for updates and enhancements.

Influence of aerosol injection on the liquid chemistry induced by an RF argon plasma jet

Ivana Sremački^{a,*}, Giuliana Bruno^{b,*}, Helena Jablonowski^b, Christophe Leys^a, Anton Nikiforov^a, Kristian Wende^b

^a*Department of Applied Physics, Ghent University, Sint-Pietersnieuwstraat 41, Gent, 9000, Belgium*

^b*ZIK plasmatis, Leibniz Institute for Plasma Science and Technology (INP Greifswald), Felix-Hausdorff-Straße 2, 17489 Greifswald, Germany*

*Both I. Sremački and G. Bruno contributed equivalently to the work

Correspondence to: kristian.wende@inp-greifswald.de and anton.nikiforov@ugent.be

Keywords: plasma aerosol, plasma jet, cysteine model, plasma liquid chemistry

Abstract:

A radio-frequency driven plasma jet in annular geometry coupled with an aerosol injection into the effluent is proposed for the controllable ROS/RNS production and delivery on biological targets in the context of plasma medicine, e.g. wound care. The role of the aqueous aerosol in modulating the reactive species production is investigated by combining physical and chemical analytics. Optical emission spectroscopy, electron paramagnetic resonance spectroscopy, and a biochemical model based on cysteine as a tracer molecule have been applied, revealing that aerosol injection shifts the production of ROS from atomic and singlet oxygen towards hydroxyl radicals, which are generated in the droplets. Species generation occurred mainly at the droplets boundary layer during their transport through the effluent, leading to a limited cysteine turnover upon introduction into the aerosol solution. The subsequent delivery of unmodified cysteine molecules at a target suggested the application of the plasma source for the topical delivery of drugs, expanding the potential applicability and effectiveness. The presence of reactive nitrogen species was negligible regardless of aerosol injection and only traces of the downstream products nitrate and nitrite were detected. In summary, the aerosol injection into the effluent opens new avenues to control UV radiation and reactive species output for the biomedical applications of non-thermal plasma sources, reaching out towards the regulation, safety, and efficacy of targeted applications.

1. INTRODUCTION

The unique feature of cold physical plasmas (CPP) to produce a mixture of highly reactive species mimicking the multi-ROS reactive oxygen species inflammatory environment is central to the plasma medicine theme. Since the first reports in the mid-nineties, showing that CPP sources can successfully inactivate bacteria the field expanded significantly [1, 2]. Numerous plasma sources were developed for the decontamination of biotic/abiotic surfaces, deposition of bioactive coatings, and manipulation of eukaryotic cells and tissues [3-5]. CPPs show several direct and indirect effects in biological models, inducing cell signaling, proliferation, apoptosis, or senescence depending on the treatment intensity (“dose”) [6]. Currently, research focuses on applications such as chronic and acute wound healing, (pre-) cancerous lesions, and other conditions involving the immune system [7-12]. The design of cold plasma sources for biomedical applications evolves in two major directions: Dielectric Barrier Discharges (DBD) [13, 14] and Atmospheric Pressure Plasma Jets (APPJ) configuration [15].

Of special interest for fundamental and biomedical practice are cold plasma reactors in direct contact with liquid since many biological samples are inevitably covered with liquid layer. Different reactor designs to study plasma-liquid interaction are developed and reviewed in [16] e.g. jets in direct contact with liquid, with liquid electrode, surface discharges, gas phase plasma with dispersed phase (aerosols) and discharges in bubbles. Introduction of liquids into electric discharges is mainly driven by the motivation to induce or enhance the plasma chemistry and change the production of reactive species OH, O[•], H₂O₂ [17]. Moreover, with introduction of aerosols into plasma, the effective interaction area between plasma and liquid increased and followed by change in species production. To modulate the interaction area and energy efficiency, a water spray has been injected into argon and air plasmas for purposes of adherent bacterial inactivation [18]. Cold RF plasma interaction with a controlled flow of micromete-size water droplets has been reported in [19], focused on the effects on droplets size and the velocity distribution after their transport through plasma ($t \sim 100 \mu\text{s}$). Moreover, detailed research on the passage of isolated micro droplet ($t \sim 10 \text{ ms}$) through cold diffuse RF plasma was reported in [20]. Accordingly, plasma-aerosol interaction represents a promising tool for quantitative fundamental studies on production of water-derived species and their controlled deposition in biological systems, underlining their importance for biomedical applications. Due to the lack of systematic studies of plasma-induced chemistry in presence of aerosols and, on the other hand, increased research interest in plasmas for biomedical application, this work is committed to the detailed study on how micro-droplets presence in effluent can change the plasma chemistry. Currently, the dispersion of droplets in the plasma effluent has been proposed for various applications in the context of plasma medicine [21]. It is well known that a range of reactive species is produced because of the plasma-liquid interaction. Further studies need to be performed on the possible applicability of aerosols as microreactors able to promote the species formation by increasing the interaction area between plasmas and liquid, possibly by-passing the physical barrier given by the plasma-liquid interface, and optimizing the delivery of the resulting chemistry on biological targets. Liquid aerosols can be devised as carrier of molecules or reactive species, and further investigations are required to substantiate the knowledge on the topic.

Accordingly, a plasma jet coupled with an aqueous aerosol spray was developed to: (i) study the variability and controllability of reactive species production and delivery on a target in presence of aerosols, and (ii) study potential roles of aerosol droplets, e.g. as carrier of reactive species, as source of reactive species, or for the delivery of drugs on biological targets. The application horizon is biomedicine, such as wound healing or cancer. The presented RF sustained annular-shaped plasma jet uses an argon working gas and operates in ambient air [22]. Its coaxial geometry allows the introduction of an aerosol into the discharge effluent. This design facilitates the direct

1
2
3 and controlled interaction of micro-droplets with the plasma effluent before reaching the (biological) target,
4 modulating the generation of active species due to a large gas-liquid interface, and open the potential to introduce
5 compounds or drugs for delivery to the target via the aerosol. Moreover, aerosol injection into the plasma effluent
6 results in a significant temperature decrease of a treated sample from 102°C to 59°C (input power 30 W) and from
7 73°C to 48°C (20 W) after 1 min treatment and a distance of 2 mm [23]. A decrease of the gas temperature by
8 10°C via the introduction of micro droplets confirming our results has been reported recently [24]. Since, a
9 thorough understanding of the physics and the chemistry of this modular source is desired to determine future key
10 points for an application both in the biomedical and in the technological scenario. So far, the biochemical potential
11 of the plasma source has not been studied in detail, especially the impact of the RF argon jet on the aerosol droplet
12 carrying organic molecules remains to be determined.

13 Besides the primary species and radiation produced in the plasma core, species that can be generated in contact
14 with air and water are of special interest for targeted applications. Among these are the reactive oxygen species
15 (ROS): superoxide $O_2^{\cdot-}$, hydrogen peroxide H_2O_2 , hydroxyl radical $\cdot OH$, singlet oxygen 1O_2 , atomic oxygen $\cdot O$,
16 ozone O_3 , and the reactive nitrogen species (RNS): atomic nitrogen $\cdot N$, nitric oxides N_xO_y , peroxyxynitrite $ONOO\cdot$,
17 and nitrous resp. nitric acid with the corresponding ions (HNO_2/NO_2^- , HNO_3/NO_3^-). The species differ in their
18 reactivity, affecting lifetime and specificity of detection. Most of them occur regularly in physiological processes
19 of living tissues, often involved in signaling processes [25, 26]. Biological reactivity of species mirrors in oxidative
20 changes of sensor molecules or – in case of excess – other biomolecules such as proteins or lipids [27]. The
21 resulting outcome is still underexplored, but it has been observed that the oxidation of proteins changes their
22 immunogenicity. In autoimmune type I diabetes patients, autoantibodies targeting experimentally oxidized insulin
23 were detected [28]. It can be assumed that the introduction of covalent modifications in biomolecules is one
24 mechanisms behind the observed biomedical effects of CPPs. Thus, the biochemical impact of a given plasma
25 source is relevant. Biomolecules such as peptides or amino acids are a suitable model to investigate the reactive
26 species produced or deposited in a target by a given plasma source and on the other hand reveal the chemical
27 structures most sensitive to the attack of reactive oxygen and nitrogen species RONS [29-32].

28 In this work, an established model system employing the amino acid cysteine as the tracer molecule has been
29 chosen to scavenge RONS generated by the RF plasma source. Cysteine is a key amino acid controlling structure,
30 location, and functionality of proteins by its different oxidation states [33]. The applicability of the model was
31 previously validated using the argon plasma jet kINPen and the helium micro-plasma COST jet [29, 32]. By
32 employing liquid chromatography and high-resolution mass spectrometry, the model can qualify and quantify the
33 major cysteine derivatives produced by the interaction with the plasma-derived species. Beside the treatment of
34 cysteine solutions with various power and distance settings, especially the direct interaction between cysteine in
35 the aerosol droplets and the plasma effluent was investigated. The chemistry occurring under different treatment
36 conditions has been clarified in presence and inside the aerosol droplets, giving insights on the applicability of
37 aerosols as source of reactive species or as carrier of drugs for topical delivery. Furthermore, electron paramagnetic
38 resonance (EPR; $\cdot OH$, $O_2^{\cdot-}$, $\cdot H$, $\cdot O$, O_3 , 1O_2), ion chromatography (IC, NO_2^- and NO_3^- ions) and a colorimetric
39 H_2O_2 assay were used to detect the deposition of short and long-lived reactive species into the liquid phase. Based
40 on these data, the mechanisms of species generation and the role of the aerosol injection on ROS and RNS
41 production are discussed.

2. MATERIALS & METHODS

In this work, a special design of argon RF APPJ coupled with aerosol droplets injection into plasma effluent region was used. Safe, stable and uniform operation of the source that is important for plasma medicine was shown in our recent work [22]. Hereby, in this work special attention is given to the effects of plasma-aerosol direct interaction on plasma efficiency of liquid media treatment. Correspondingly, varieties of diagnostic techniques were applied to support the study on chemical characterization of the source operation in ambient air with and without an aerosol. Optical emission spectroscopy (OES) and Fourier transform IR spectroscopy (FTIR) have been used to give insight into the composition of species in the plasma gas phase and plasma-aerosol medium. In next step, the treated liquid target was analyzed in terms of liquid-chemistry with colorimetric assays, ion chromatography (IC), and electron paramagnetic resonance (EPR) spectroscopy, with focusing on a model of cysteine oxidation in presence of plasma and plasma in contact with the aerosol.

2.1 Design of the plasma discharge

The plasma reactor was constructed in a geometry to allow introduction of aerosol droplets in the effluent. Plasma jet in annular shape 1 mm thick with external diameter $d_{\text{ex}}=14\text{mm}$ was generated in coaxial hollow-electrode geometry. RF powered inner electrode was made of corrosion-resistant stainless steel, while an external grounded electrode was made of aluminum. All experiments were carried out for two applied powers further indicated as “low” $P=20\text{ W}$ and “high” $P=30\text{ W}$. Low and high power settings correspond to dissipated power in the discharge of 8 and 12 W respectively, as estimated in our previous publication [22]. The high power is a maximum discharge power when RF plasma exists in α mode of operation. In operational range reported here, gas temperature in plasma effluent was $330 (\pm 15)\text{ K}$ for 20 W and $350 (\pm 15)\text{ K}$ for 30 W, while electron temperature and density were previously estimated to be 1 eV and $3.2 \cdot 10^{18}\text{ m}^{-3}$ [22]. On a top of the reactor, a NexTgen ultrasonic spraying nozzle was installed (**Fig. 1a**). Plasma forming gas argon was fixed at 3 standard liter per minute (slm) corresponding to maximal gas velocity in the effluent of 1.4 m/s. The flow rate was previously verified to generate uniform diffuse discharge in α -regime in a laminar gas flow regime (**Fig. 1b**). The flow rate of aerosol liquid to be sprayed was controlled with a syringe pump at a flow of 0.1 mL/min. The optimal value of flow rate was chosen, assuring a uniform and reproducible spray during a treatment time between 10 and 60 s. The aerosol was injected into the effluent and did not pass through the active plasma that is formed between the electrodes (**Fig. 1**). The mean size of the aerosol droplets was $22 (\pm 0.825)\ \mu\text{m}$, determined based on the datasheet provided by the company SinapTec, NexTgen Ultra Sonic platform. Additionally, 1 slm flow of Ar gas was applied through the central electrode to push droplets downwards with a velocity of 0.2 m/s to prevent aerosol condensation inside of the plasma source during the treatment time and formation of large droplets due to condensation. The axial image of the plasma ring has been presented in our previous work [22], nonetheless taking the same axial image of plasma ring with introduced aerosol droplets would be impossible as aerosols would block the optical access resulting in unclear image upon its condensation.

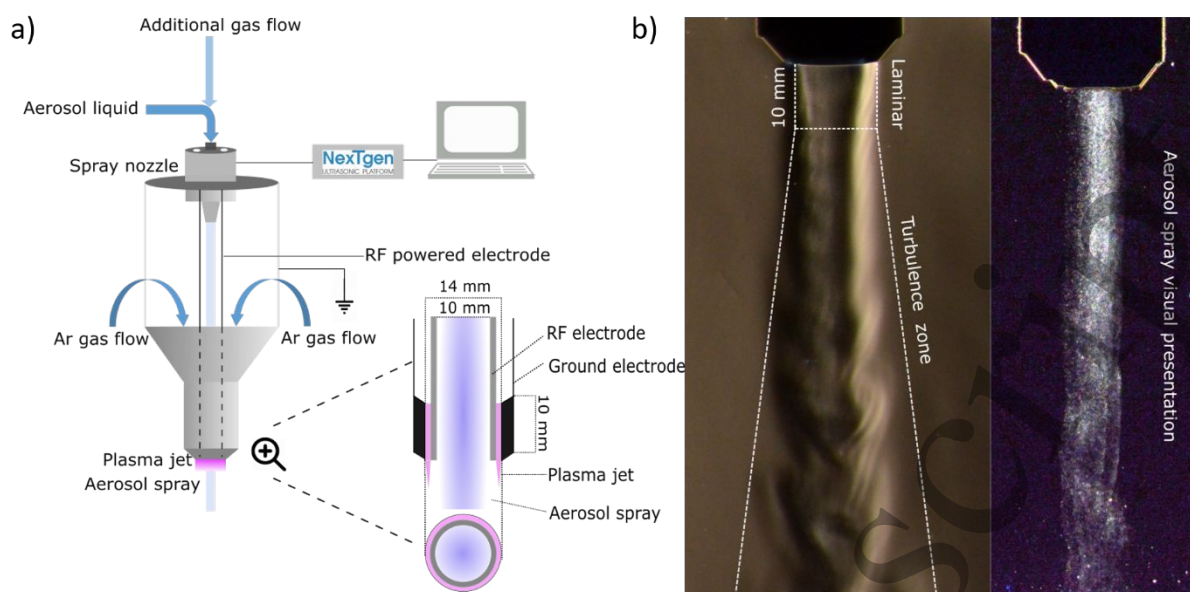


Figure 1. a) General view of the plasma jet reactor with aerosol injection and enlarged cross section of the nozzle, b) Visual view of the gas flow obtained by Schlieren imaging indicating two zones of different gas flow regime (on left) and visual view of the aerosol spray (on right).

2.2 Spatial resolved optical emission spectroscopy (OES)

Optical emission spectroscopy can be used as a qualitative method to give insight into the composition of excited species present in plasma. Emission from excited species in plasma effluent has been measured in the range of 250-900 nm. The Ocean Optics spectrometer with the resolution of 1.7 nm was used to record emission spectra from the plasma effluent. Spectral sensitivity of the spectrometer, transparency of the fiber and collection optics were calibrated with an Oriel model 63355 quartz tungsten-halogen lamp. The light emitted by the plasma effluent was collected with a fiber ($d=200\ \mu\text{m}$) located 2 mm away from the region of interest resulting in an acceptance angle corresponding to the spatial resolution of 1 mm. This arrangement of the spectral measurements prevents collection of the radiation from the discharge region and ensure that only light emission from the effluent was recorded. Line-of-sight measurements were performed to record spectra for 3 positions perpendicular to the axis of the jet, 2 mm from the nozzle in visible plasma effluent, 6 mm from the nozzle and 8 mm away from the nozzle – far effluent. The effluent was imaged using an Hamamatsu ICCD camera ($5\ \mu\text{s}$ exposition, 1000 integration), coupled to bandpass filters with a transparency of 10 nm full width at half maxima FWHM centered at 751 and 298 nm corresponding to Ar I and OH(A-X) emission, respectively.

2.3 Fourier-transform infrared spectroscopy (FTIR) analysis

FTIR high-resolution spectroscopy was performed with the use of Matrix-MG2 spectrometer of $0.5\ \text{cm}^{-1}$ resolution in order to detect and estimate the absolute concentration of the most abundant long-living compounds generated in the gas phase with and without the aerosol. The spectrometer coupled with multi-pass cell of 5 m was calibrated for H_2O , N_2O , N_2O_5 , NO , NO_2 , O_3 compounds with a sensitivity of 0.1 ppm. Gas from the plasma was directed in a tube through which dry air was circulating in flow range 0.5-1 SLM, in order to simulate an open atmosphere operation. Once aerosol was introduced in the plasma, trapped gas was filtrated through a quartz wool to reduce water droplets entering the FTIR system to a minimum while having only limited impact on the detected RONS.

In pilot experiments, filtering was found unavoidable. To minimize the effect of quartz wool all experiments were performed after reaching steady state ($T=5$ min). The FTIR spectra were averaged 30 times in progression mode and recorded in the wavenumber range of $800\text{-}6200\text{ cm}^{-1}$.

2.4 Samples preparation and plasma treatments of liquids

For mass spectrometry analysis, 1 mM solutions of cysteine amino acid (L-Cysteine, Sigma Aldrich) were prepared fresh daily. The pH was stabilized at pH 7.4 by the use of 5 mM phosphate buffer (HPLC-MRM analysis) or 5 mM ammonium formate (direct infusion shotgun HRMS). For electron paramagnetic resonance (EPR) experiments, the spin trap / spin probe was solubilized in 5 mM phosphate buffer. In pilot experiments, a volume of 1.5 ml sample in a 6-well plate was determined to be optimal.

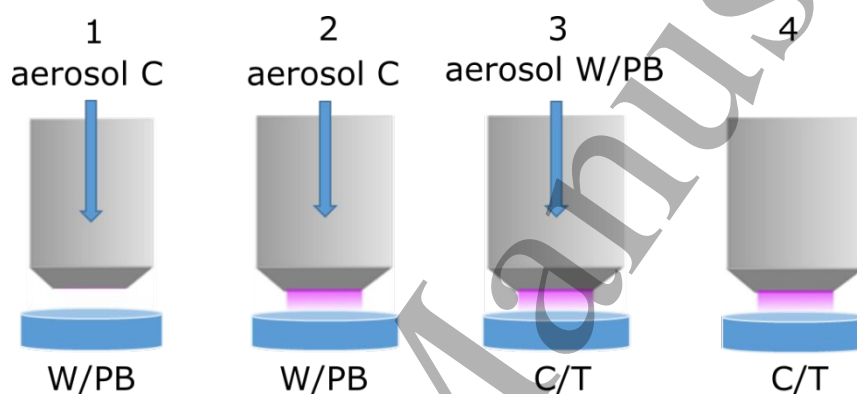


Figure 2. General experimental setups. Ultrasonic aerosol used in setups 1 to 3. Plasma off conditions (setup 1) used as background control. Abbreviations: C for cysteine, T for trapping trap/spin probe, W for water, and PB for phosphate buffer

Cysteine oxidation was investigated for plasma power of 20 and 30 W, treatment time variation (10, 35, 60 s) and distance variation of target from the effluent (2, 6, 12 mm). Target was the treated (and tracer-enriched) liquid collected for chemical analysis, namely mass spectrometry, EPR, IC and colorimetric assays. Treatment time reported in this work is the exposure time of a plasma treatment of 1.5 mL liquid sample by the setups shown in Fig.2. Four different set-ups including or excluding aerosol injection were used (Fig. 2/Tab. 1). For some experiments, the aerosol was generated from a 1 mM cysteine solution and collected for analysis into either empty well plates or wells filled with 1.5 mL water with estimated dilution and final concentrations $c=11\text{ }\mu\text{M}$, $c=37.5\text{ }\mu\text{M}$ and $62.5\text{ }\mu\text{M}$ during 10, 35 and 60 s treatments. Evaporation of the aerosol droplets in the effluent was not taken into account, since imaging showed a negligible effect in the considered distances (see Fig. 1.b). However, droplets may partially be evaporated during the transport to the treated liquid. Correspondingly, the chemical analysis performed in this work represents the integral effect of droplets and gas phase water molecules on the plasma-induced chemistry. Overall aerosol loss due to evaporation in the effluent on the distance up to 15 mm from the nozzle has been estimated low as can be seen from the almost constant intensity of the visible aerosol jet Fig. 1b.

Table 1. Overview of the plasma treatment protocol. PBS = phosphate buffered saline; spin trap/spin buffer = 2 mM BMPO or 100 mM TEMPD (see figure 2)

Set-up	Aerosol liquid	Target liquid	Power (watt)	Distance (mm)	Treatment time (s)
1	1 mM cysteine in water (C)	water (W) or phosphate buffer (PB)	0 (control)	2, 6, 12	10, 35, 60
2	1 mM cysteine in water (C)	water (W) or phosphate buffer (PB)	20, 30		
3	water (W) or phosphate buffer (PB)	1 mM cysteine in water (C) / spin trap in PBS (T)			
4	No aerosol	1 mM cysteine in water (C) / spin trap in PBS (T)			

The aerosol injection into the plasma effluent considerably changed the surface area of the effluent/liquid interaction. Knowing that mean diameter of the aerosol spherical droplet is 22 μm , calculated mean volume and surface of the droplet are respectively 5575 μm^3 and 1520 μm^2 . Assuming a droplet mean volume and the flow rate of aerosol liquid 0.1 mL/min (1.66 $\mu\text{L/s}$) estimated droplet formation rate is 3×10^5 droplets/s. Subsequently, the effective interaction area of droplets with the plasma effluent was calculated to be 4.5×10^3 , 1.6×10^4 , and 2.7×10^4 mm^2 for the treatment of 10, 35, and 60 s, respectively. It has to be noted that aerosol droplets interact with plasma only during a short time when passing through the effluent (2 mm or 10 ms). In comparison, an area of up to 500 mm^2 is treated in condition 4 (6-well plate, 2 mm distance). Despite the laminar flow along of the first 10 mm after the nozzle, of both plasma feeding gas Ar with velocity 1.4 m/s and flow of aerosol droplets with velocity 0.2 m/s, once the target is placed under the nozzle laminar regime cannot be verified. Placing the liquid target in the direction of gas and droplets flow strongly perturbs the flow dynamics resulting in switching to turbulent behaviour and effective mixing of the effluent with droplets in the region between the nozzle and liquid target. Unfortunately, the actual number of the droplets coming in contact with plasma effluent and interacting with effluent is very hard to estimate. This would involve experimental PIV (Particle Image Velocimetry) laser technique or particle tracing simulation in COMSOL modelling platform which is out of scope of current work.

2.5 High-Pressure Liquid Chromatography & Mass Spectrometry (HPLC-MS)

Qualitative high-resolution mass spectrometry analysis was achieved by direct infusion of the cysteine solutions into a TripleTOF 5600 (Sciex, Darmstadt, Germany). 10 $\mu\text{L/min}$ of solutions were infused using a Turbo V ion source, using optimized parameters (negative polarity, curtain gas 35 psi, gas1 20 psi, gas2 25 psi, capillary temperature 150 $^\circ\text{C}$, spray voltage 4.5 kV). The spectra were acquired in a mass range of 30 to 400 mass to charge ratio (m/z). Quantitative analysis was achieved by high-pressure liquid chromatography – mass spectrometry coupling. An Infinity II 1290 system (Agilent Technologies, Waldbronn, Germany) was equipped with a HILIC 2.1 mm x 100 mm Acquity Amide Column (130 \AA pore size, 1.7 μm particle size, Waters, Manchester, United Kingdom) and a respective pre-column (2.1 mm x 5 mm). Using 400 μL flowrate and an 18 min gradient of A (10 mM ammonium formate plus 0.15% formic acid in water) and B (85% acetonitrile, 10 mM ammonium formate buffer pH 3) the baseline separation of cysteine, cystine, cystine sulfonic acid, and cysteine-S-sulfonate was achieved (Sigma, Deisenhofen, Germany). The details of the gradient are resumed in **Table S1**. A qTRAP 5500 triple quadrupole instrument (Sciex) was used in Multiple Reaction Monitoring (MRM) strategy for detection and quantification. All compounds were analyzed in positive ion mode, and specific transitions were monitored in the

MRM experiments (**Table S2**). External calibration curves were prepared. All samples were injected or infused twice (technical duplicates).

2.6 Electron paramagnetic resonance spectroscopy (EPR)

Spin trap enhanced electron paramagnetic resonance spectroscopy (EPR, EMXmicro, Bruker Biospin GmbH; X-band 9.75 GHz; magnetic field up to 0.65 T) using the Xenon software in addition with the spin counting module (Bruker Biospin GmbH) was applied to quantify radicals/reactive oxygen species. The following instrument parameters were used: modulation frequency 100 kHz, modulation amplitude 0.1 mT, microwave power 5.024 mW, receiver gain 30 dB, and a time constant of 0.01 ms. 5-tert-Butoxycarbonyl-5-methyl-1-pyrroline-N-oxide (BMPO, Dojindo Laboratoire, Japan) – a spin trap for $\cdot\text{OH}$, $\text{O}_2\cdot^-$, $\cdot\text{H}$, was dissolved in 5 mM phosphate buffer to a final concentration of 2 mM, and 2,2,6,6-tetramethyl-4-piperidone (TEMPD, Sigma Aldrich) – spin probe for $\cdot\text{O}$, O_3 , $\text{O}_2(\text{a}^1\Delta_g)$, was dissolved in the same system to a final concentration of 100 mM. For all experiments, an untreated sample was measured prior to the plasma treatment. More details on the measurement procedure can be found in [34-37].

2.7 Hydrogen peroxide assay

Hydrogen peroxide (H_2O_2) was detected via a colorimetric assay. 10 μL of sample were incubated for 15 minutes with 100 μL of reagent, consisting in a solution of xylenol orange, sorbitol and ammonium ferrous (II) sulfate (Pierce™ Quantitative Peroxide Assay Kit, Thermo Scientific). In aqueous solutions, sorbitol and hydrogen peroxide react to form peroxy radicals, which oxidize Fe^{2+} to Fe^{3+} . This induces a color change of xylenol orange, detectable at 595 nm through a spectrophotometer (Infinite M200 Pro plate reader, Tecan, Männedorf, Switzerland). Each sample was analyzed in triplicate. The assay delivers a linear response between 0.78 and 50 μM H_2O_2 , and the concentration of H_2O_2 could be determined safely starting from 2.3 μM .

2.8 Ion chromatography (IC)

Nitrite (NO_2^-) and nitrate (NO_3^-), as well as sulfite (SO_3^-) and sulfate (SO_4^-), were quantified via ion chromatography (ICS-5000, Thermo, Dreieich, Germany). For separation a weak ion exchange column (IonPac AS23 2 x 250 mm) and respective precolumn (2 x 50 mm IonPac AG23) was used (Thermo Scientific). The ions were separated in 25 min isocratic run, at a flow rate of 0.25 mL/min, using 80 mM HCO_3^- and 450 mM CO_3^{2-} buffer as mobile phase. External calibration curves were measured for all ions using the Seven-Anion standard (Dionex/Thermo Scientific) or sodium sulfite analytical standard (Sigma Aldrich, Deisenhofen, Germany). Each sample of three different experiments was injected in duplicate.

3. RESULTS & DISCUSSION

3.1 Active species generation in the effluent

To stabilize the plasma properties as well as sustainable power when dealing with plasma in contact with liquids, introduction of an aerosol in the effluent and not directly in the discharge between the electrodes is beneficial. It has to be highlighted that the introduction of the aerosol into plasma effluent does not affect the discharge properties. Spatially resolved emission spectroscopy results for the plasma effluent in three different positions 2, 6 and 8 mm from the nozzle, in pure argon plasma and plasma in contact with aerosol, are shown in **Fig. 3**.

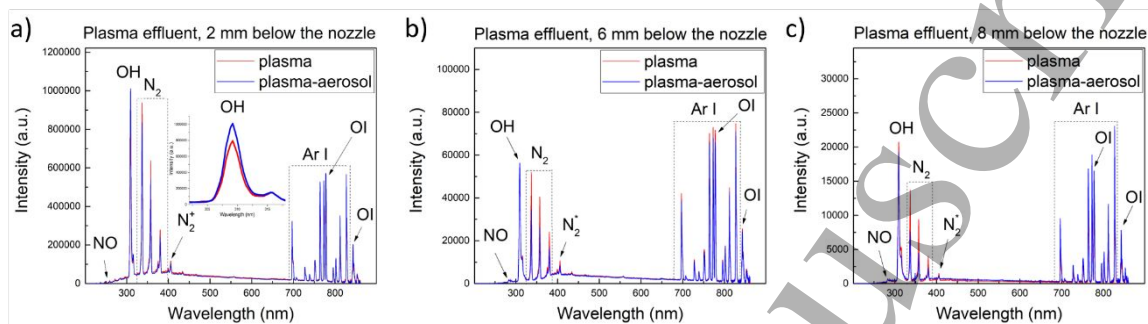


Figure 3. Overview of Ar plasma jet emission without the use of aerosol (red) and plasma emission when in contact with aerosol (blue) in a range of 250-900 nm in the effluent positions corresponding to a) 2 mm, b) 6 mm and c) 8 mm below the nozzle, $P=30\text{W}$

The effluent emission in ambient air mainly consists of radiation of excited species Ar I, O I, OH(A-X) radicals, and N_2 (C-B) as marked in Figure 3. However, weak emission from NO molecules has been also detected below 300 nm. The observed continuum appearing in the region 300-600 nm is ascribed to the Bremsstrahlung radiation and NO_2 chemiluminescence as explained in details in our work on similar RF discharge operating in a planar geometry [38]. All spectra were recorded along effluent where interaction of aerosol with effluent took place. Emission intensity was highest in close vicinity to the nozzle (**Fig. 3a**) and exponentially decreased with the distance. In argon plasmas operating under ambient conditions, the energy transfer from Ar^* to N_2 is an important and effective process and it can be used as an indicator of plasma interaction with air. Energy transfer is expected to be high as soon as excited Ar atoms leave the active plasma volume and collide with surrounding air corresponding to a case presented in **Fig. 3**. In all three positions (**Fig. 3**) entrance of N_2 in the plasma effluent can be seen and consequently its excitation. Presence of the aerosol in the effluent leads to an increase of OH radicals emission intensity more than 25% in position closest to the nozzle, indicating a probable increase in OH radicals production by water aerosol injection (see the inset in **Fig. 3a**). The intensity of NO excited molecule emission is higher in Ar plasma without aerosol. In addition to a changed formation of NO due to gas phase chemistry, a partial absorption of NO emission as reported for UV radiation below 300 nm [39] and direct quenching of NO radicals could not be excluded based on the OES measurements and may result in an underestimation in this condition.

The plasma chemistry in the far effluent, especially when aerosols are introduced is mainly driven by VUV/UV radiation generated in plasma between electrodes and emitted in the direction of gas flow. The VUV/UV emission has been recorded for the active plasma zone (**Figure 4**). As expected in argon driven plasmas, argon excimers Ar_2^* on 126 nm and atomic oxygen OI 130 nm radiation is dominating VUV/UV spectra of the plasma. It has to be emphasized that due to the high abundance of monoatomic gas Ar respect to the ambient air in the direction of the emission detection, VUV/UV photons are detected far as 12 mm from the edge of the visible effluent (14 mm

from the electrode). As VUV/UV spectra have been recorded only axially from region between the electrodes and no UV emission has been detected from the plasma effluent, aerosol effect on UV emission has been not considered due to technical limitations. Namely, simultaneous spraying of aerosol on the UV spectrometers window and detection of UV radiation would lead to the condensation and formation of liquid layer on the spectrometers window and consequent absorption. It has been reported in [39] that excimer radiation emitted at 126 nm will be absorbed by 99% in water layer thin as 4.6 μm based on Lambert-Beer law, while experimentally 50% absorption has been measured in 200 μm water layer for photons $\lambda < 180 \text{ nm}$. Taking into account the average aerosol droplet size $d = 22 \mu\text{m}$, high energy photon encountering aerosol droplet on its way to the detection system is very unlikely to detect.

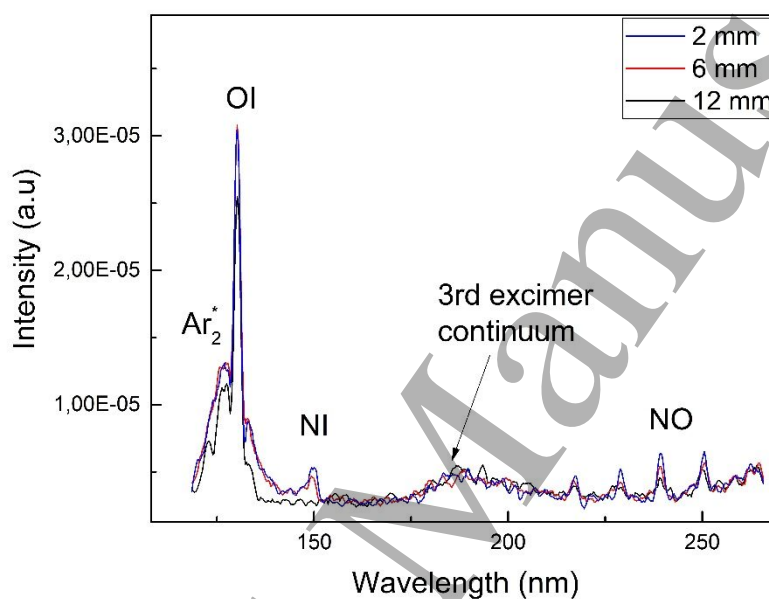


Figure 4. VUV/UV spectra of annular shape plasma jet recorded from active plasma zone (inter-electrode region) for three distances from the edge of the visible effluent: 2 mm (blue), 6 mm (red) and 12 mm (black), working power $P = 30 \text{ W}$

To examine potential changes in plasma dynamics behavior and plasma radiation with aerosol injection into plasma effluent, the effluent has been imaged for Ar I and OH emission using ICCD, keeping in mind that the significance of the data can be challenged since the presence of the droplets may result in quenching effects. Additionally, both optical techniques do not give information about absolute densities of the observed species. Despite some noticeable changes in OES revealed in case of aerosol injection, an overall impact of the aerosol on the discharge effluent is relatively weak and mostly attributed to drop in Ar I lines and increase of OH emission. The low impact of the aerosol was also confirmed by the effluent imaging presented in **Fig. 5** for both Ar I and OH (A-X) emission. In both conditions, with and without aerosol injection, the profile of the radiation is very similar that indicates a low impact of the aerosol on excited species production that well agrees with OES results. Visible emission of the effluent at 750 nm and 280 nm is detected only 1 mm below the nozzle (**Fig. 5**) what can be assigned to low signal to noise ratio of the camera $\text{SNR} = 10$. It ensures that during the experiments that no direct interaction of the plasma with treated media and effect of electrons or charged species on liquid chemistry in the absence of the aerosol can be neglected.

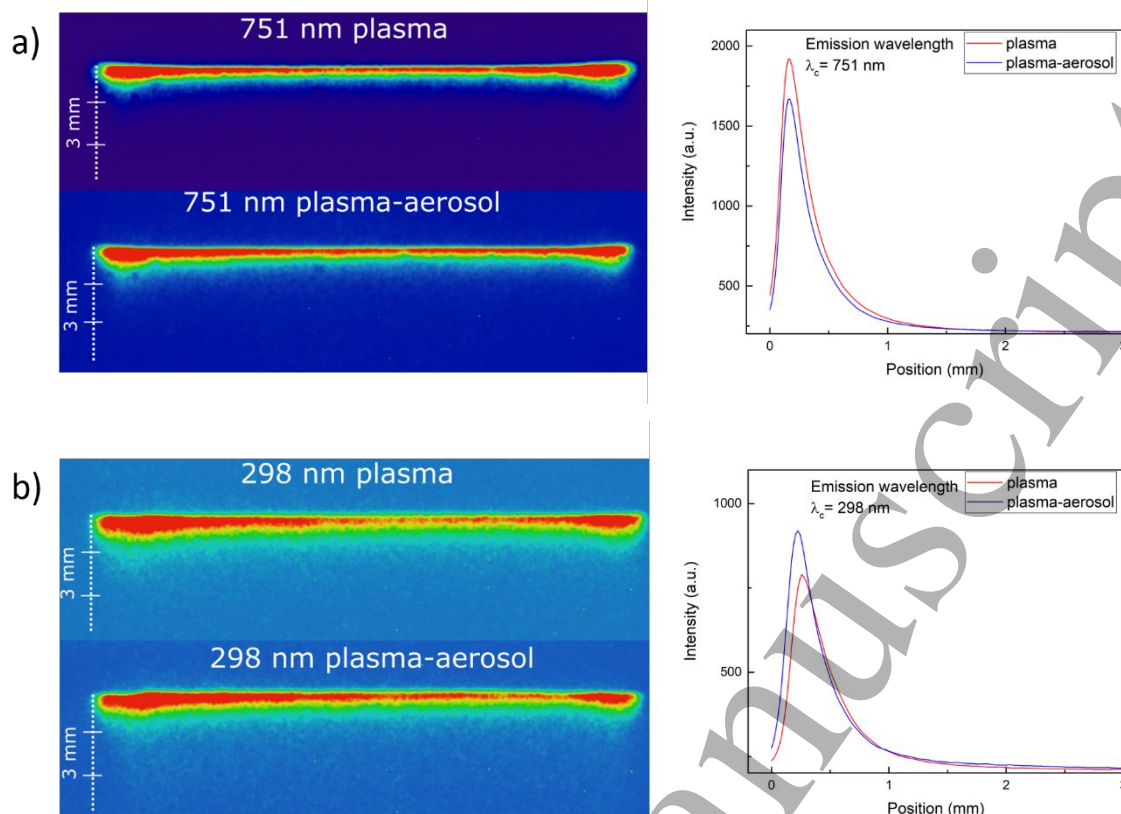


Figure 5. Plasma effluent imaging at two different wavelengths : a) 751 nm (Ar I emission); b) 298 nm (OH emission) at RF input power $P=30$ W

With the use of FTIR a low production of ozone, below 20 ppm in the gas phase, was confirmed for all plasma and plasma-aerosol conditions. FTIR spectra of Ar jet and jet in contact with water aerosol under operating power 20 W are presented in Fig. 6. Rotationally resolved spectra of water molecule bending vibrations $1400\text{--}2000\text{ cm}^{-1}$, and stretching vibration $3600\text{--}4300\text{ cm}^{-1}$, $5100\text{--}5600\text{ cm}^{-1}$ are dominant in all conditions, while ozone peak located at 1051 cm^{-1} , can be also seen in Ar plasma after 5 minutes of operation. In argon plasma without aerosol, a simultaneous decrease of water content and an increase of ozone has been noted from $c(\text{H}_2\text{O})=400$ ppm and $c(\text{O}_3)=1.04$ ppm to $c(\text{H}_2\text{O})=230$ ppm and $c(\text{O}_3)=9.5$ ppm at 20 W RF power after 5 minutes of operation. At the water concentration of $c(\text{H}_2\text{O})=400$ ppm a significant change in plasma chemistry as reported in [40] was expected and therefore a stabilization phase of 5 minutes of operation was applied before measurement. High amount of H_2O at the beginning of experiments was attributed to adsorption of water vapor on gas Teflon tubes and metal body of the jet that is decreasing during the operation. In addition, access of ambient atmosphere to the reactor when not in use allowed a potential adsorption of water on the electrodes. Gas temperature and wall temperature were close to the room temperature (~ 300 K) and no substantial heating of the device due to the presence of plasma has been noticed. During the measurement, a slow removal of the absorbed water from the walls due to the presence of gas flow occurs. Gas temperature effect on water concentration is negligible and there is very little gas heating in this device. At higher RF power of 30 W higher $c(\text{O}_3)=12.7$ ppm was observed after 5 minutes of operation indicating positive effect of the discharge power on O_3 production. This trend was not observed when aerosol was introduced: the humidity of the trapped gas was significantly higher $c(\text{H}_2\text{O})=1175$ ppm increasing to $c_2(\text{H}_2\text{O})=1500$ ppm during the same time of 5 min, while ozone concentration was constant at $c(\text{O}_3)=3.5$ ppm. The

observed lower concentration of ozone in the case of aerosol introduction is very probable due to quenching of O atoms (precursor of O₃ production) by H₂O with formation of OH radicals. No presence of any traces of N_xO_y products was revealed which is well agreed with OES results where both NO and NO₂ peaks were very weak, see **Figure 3**. This observation indicates that generation of nitrogen reactive species in RF plasma operation in air with and without aerosol is very ineffective and can be neglected in the analysis of the plasma-initiated chemistry in liquid target.

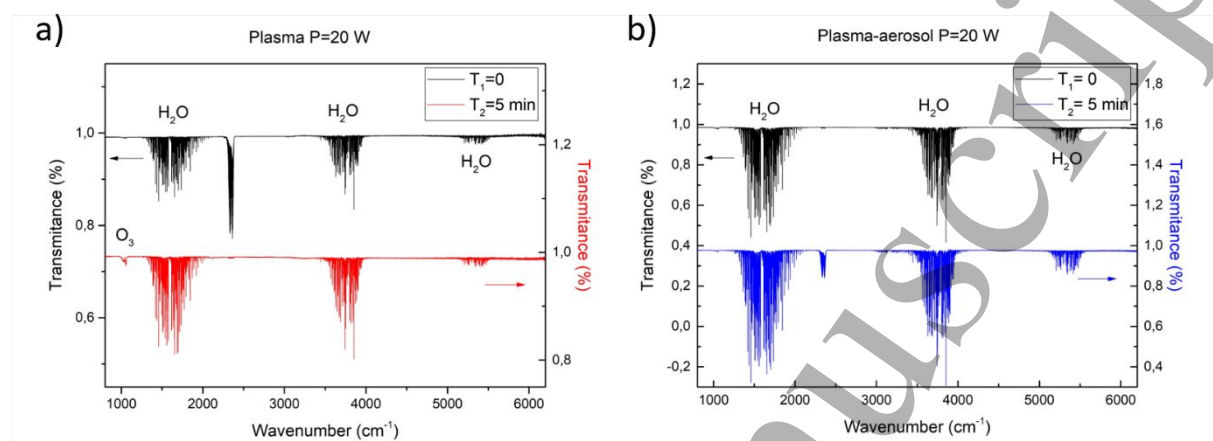


Figure 6. FTIR spectrum in range 800-6200 cm⁻¹ of: a) argon plasma jet, b) plasma jet in contact with aerosol at power P=20W.

3.2 Deposition/production of RONS in treated liquids

Due to the importance of plasma-induced chemical process in liquid media for biomedical applications, a chemical analysis of RONS in liquid was performed. Short-lived reactive species, such as atomic oxygen ([•]O), singlet oxygen (¹O₂), ozone (O₃), hydroxyl radicals ([•]OH), superoxide anion radicals ([•]O₂⁻), and hydrogen radicals ([•]H) were analyzed via EPR. The deposition of long-lived reactive species in the treated liquid target was investigated by ion chromatography (nitrite, NO₂⁻ and nitrate, NO₃⁻), and a colorimetric assay (hydrogen peroxide, H₂O₂).

3.2.1 Short-lived reactive species

Using BMPO as a spin trap, hydroxyl radicals ([•]OH), superoxide anion radicals (O₂^{•-}), and atomic hydrogen ([•]H) were detected in the liquid target, after treatments with plasma and plasma-aerosol (**Fig. 7**). The measured concentrations of BMPO-OH represents ~ 0.6% of the accumulated hydroxyl radical concentration during the treatment according to the published trapping efficiencies [41], and 90% of the less reactive and more easily trapped superoxide anion radical (BMPO-OOH) [42]. For the hydrogen atoms (BMPO-H), no trapping efficacy for BMPO is reported. Given a similar lifetime in gas phase, a trapping efficacy similar to OH radicals may be assumed. Therefore, significant amounts of hydroxyl radicals ([•]OH) and hydrogen atoms were detected, along with considerably lower amounts of O₂^{•-}. In **Fig. S1**, the measured BMPO peaks and the different simulated BMPO-adducts for treatment with and without the presence of the aerosol after 60 s plasma treatment and for a distance of 12 mm are shown.

Interestingly, the observed species concentrations as a function of treatment time and distance are similar, suggesting a common origin of the three species. All three radicals can be formed most likely by the interaction of water molecules with gas phase species, such as Ar excimers [43-46], radicals (e.g. [•]O) or ozone decay products [47-49]. However, ozone formation is not favored in the discharge, as FTIR data showed trace amounts only. In

Fig.4. VUV/UV emission from the plasma ring has been presented as a function of the distance from the nozzle to the optical detector. Interestingly, in the direction of the gas flow, high level of VUV emission from Ar_2^* , O I and N I states has been still detected on the longest distance of 12 mm, suggesting an important role of VUV radiation on plasma driven liquid induced chemistry at long distances to the target. Namely, photolysis of the water can be induced by radiation from plasma below 180 nm originating from argon excimers Ar_2^* ($\lambda=126$ nm), atomic oxygen O I ($\lambda=130$ nm) and nitrogen N I ($\lambda=149$ nm) and can be responsible for formation of ROS in liquid phase. In the presence of the aerosol, a slightly lower deposition of $\cdot\text{OH}$, $\text{O}_2^{\cdot-}$ and $\cdot\text{H}$ in the liquid bulk was observed, pointing towards the aerosol droplets acting as scavenger partner for high reactive/energetic species. Especially (V)UV radiation below 180 nm, leading to the photolysis of water because of intensive radiation of Ar_2^* excimers and O I and N I emission, is absorbed due to the presence of the droplets. Similarly, the generation of other species is quenched due to the large effective interaction-area of the aerosol droplets with the effluent in comparison to a treated liquid bulk (see 2.4). The effect of UV radiation above 200 nm on liquid chemistry is considered to be low with and without aerosol due to water transparency for such radiation and low level of emission in that region (see Fig.4 region 200-300 nm). Since no spin probes were injected by the aerosol route, these OH radicals were lost to recombination and other secondary reactions and did not contribute to the EPR signals of the liquid bulk, leading to its reduction in the presence of the droplets. This indicates that the de-novo formation of species occurs mostly at the gas-liquid interface of droplet or bulk liquid, outcompeting the deposition of species formed in the gas phase. This assumption is supported by previous works, where $\cdot\text{OH}$ formed in the gas phase due to presence of humidity was not transported in the liquid [50, 51]. Alongside, a transport of $\cdot\text{H}$ and $\text{O}_2^{\cdot-}$ by the droplets to the liquid bulk was not observed and the species decayed before reaching the spin traps/spin probes.

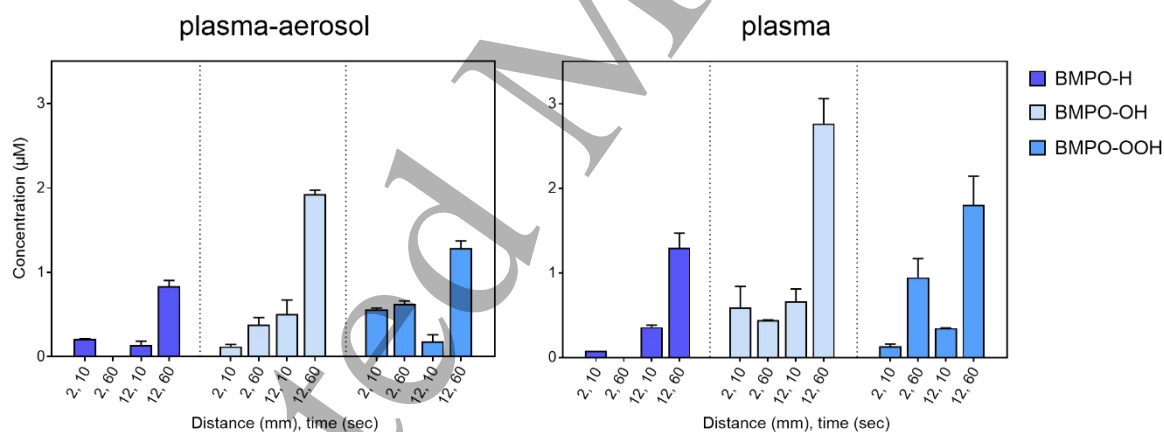


Figure 7. BMPO-adduct concentrations after plasma/plasma-aerosol treatment for 10 and 60 s, 1.5 mL water, at 2 and 12 mm distance. RF power of 30 W (setups 3 and 4). Trapping efficiencies are not considered (H unknown, $\cdot\text{OH}$ 0.6 %, and $\text{O}_2^{\cdot-}$ 90 %)

To obtain further insight, the deposition of O_3 , $^1\text{O}_2$, and $\cdot\text{O}$ were measured using TEMPD. In contrast to BMPO, TEMPD is a spin probe, which means it is reacting with reactive species without binding the species to itself, and therefore, it is not giving a characteristic spectrum for different species and identification is not possible [35, 52]. However, when considering the species different lifetimes, useful information could be obtained. In **Fig. S2**, the detected and simulated peaks of the TEMPD-adduct are given for 60 s and 2 mm treatment distance.

In contrast to the BMPO-adducts, the detected concentrations decreased with increasing treatment distance and increased with treatment time (**Fig. 8**). For 12 mm distance, no signal was detected indicating that long-lived ozone

is not relevant for this plasma source. Since the formation of O_3 takes place via a three-body reaction of O_2 and $\cdot O$ with a third partner [35, 53], the concentrations usually increase with higher distances [35, 54]. However, as shown by FTIR spectroscopy data (Section 3.2), the ozone formation in the gas phase was low (12.7 ppm maximum with an applied plasma power of 30 W), probably due to low density of molecular oxygen in the effluent required for O_3 production [55].

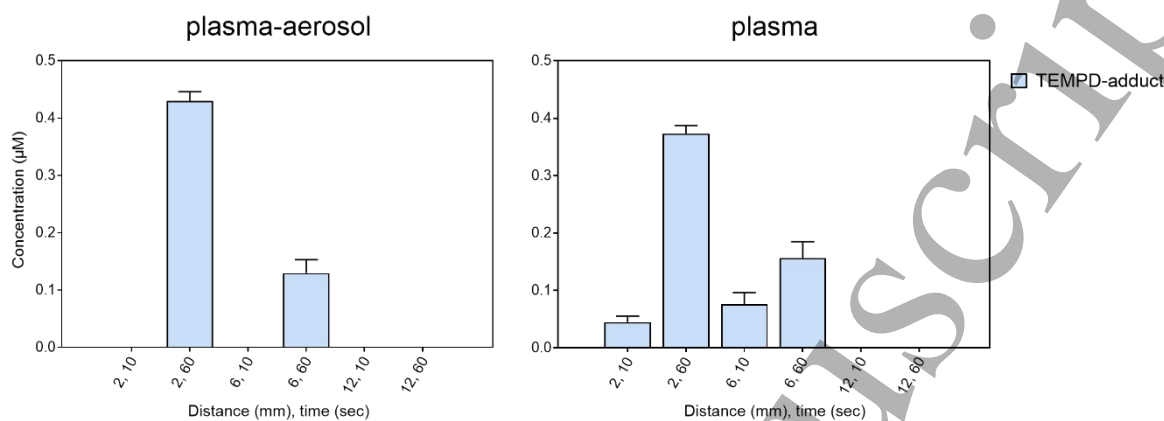


Figure 8. TEMPD-adduct concentrations for the detected species after different treatment times (10, 60 s) for 2, 6 and 12 mm with and without the aerosol presence, setups 3 and 4 respectively.

In contrast, signals at 2 and 6 mm show the presence of short-lived atomic ($\cdot O$) and/or singlet oxygen ($O_2(a^1\Delta_g)$) that are exclusively generated in the gas phase, via a reaction between argon metastables and O_2 [53, 56, 57]. Atomic oxygen is highly reactive and reacts with $\cdot OH$, yielding $HO_2\cdot/O_2\cdot$ [51], or with H_2O yielding two $\cdot OH$ radicals. It has a short lifetime under ambient atmosphere conditions, and is quickly quenched forming molecular oxygen and ozone. This explains the absence of TEMPO active ROS for 12mm distance and a small but detectable amount of product for 2 and 6 mm and 10 s treatment in dry/non-aerosol conditions. Indeed, the presence of aerosol could scavenge the deposition of $\cdot O$ by interacting with the water droplets in the gas phase [58, 59]. The second (less abundant) candidate responsible for the EPR signal of TEMPD in both plasma with and without aerosol is $O_2(a^1\Delta_g)$. The slight increase of TEMPD-adduct in the presence of the aerosol may suggest a transport of $O_2(a^1\Delta_g)$ in the aerosol droplets when distances and transfer times are short (2 mm \approx 10 ms), however, given the lifetime of 20 μs the contribution of the transport is limited.

3.2.2 Long-lived reactive species

The long-lived reactive species hydrogen peroxide (H_2O_2), nitrite (NO_2^-), and nitrate (NO_3^-) were quantified (Fig. 9). Nitrite and nitrate can be considered final stable products of the short-lived nitrogen species, such as peroxyxynitrite, NO , or NO_2 radicals [36, 37]. In the same way, hydrogen peroxide, an almost ubiquitous product of cold plasma discharges formed e.g. by the recombination of OH radicals or disproportionation of superoxide anion radicals [36, 37]. The deposited amount of H_2O_2 was significant, also in comparison with other plasma sources [29, 60], reflecting an intensive production of OH radicals in gas and/or liquid phase. In contrast, the deposition of nitrite and nitrate was below the average, indicating a strong dominance of oxygen species, which is in agreement with the FTIR results. The presence of aerosol reduced the deposition of NO_x^- ions further, indicating

that primary species, namely N_xO_y molecules, are generated in the plasma region and not in the plasma/aerosol droplets interface. Additionally, the low solubility of N_xO_y in aqueous media contributes to the observation. The presence of the aerosol suppressed the deposition of H_2O_2 significantly in comparison to plasma only treatments. In presence of the aerosol, an increased deposition with time was observed while in its absence an inverse relationship appeared. This decay of H_2O_2 in plasma-only conditions could be due to (V)UV radiation-driven photo-dissociation in liquid or the reaction of H_2O_2 with atomic oxygen at the interphase. The argon specific excimer around 126 nm emits UV radiation capable of cleaving H-O bonds. For longer distances, deposition decreased due to the lifetime of the precursor species OH and O_2^- and decay and competitive reactions occur.

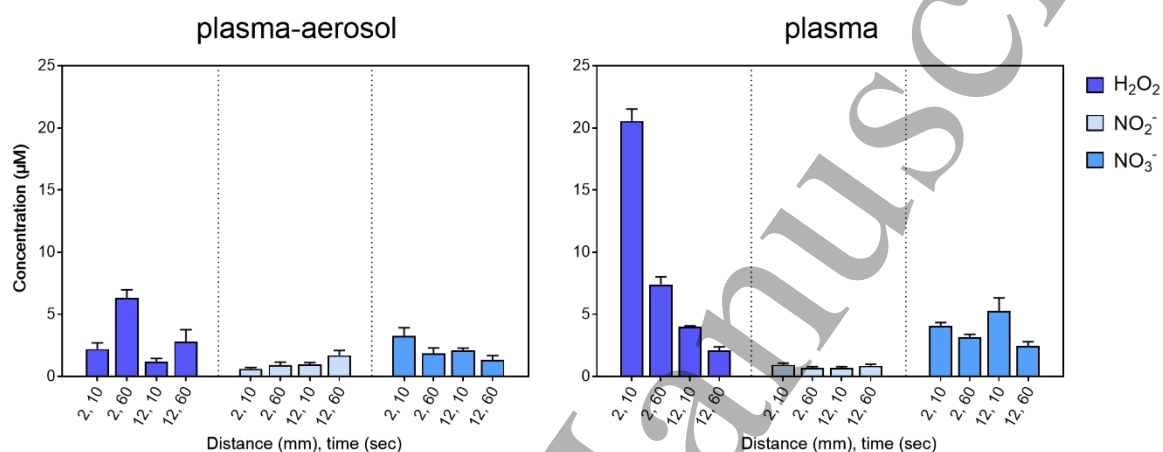


Figure 9. Hydrogen peroxide (H_2O_2), nitrite (NO_2^-) and nitrate (NO_3^-) concentrations for the detected species after different treatment times (10, 60 s) for 2 and 12 mm with and without the aerosol presence, setups 3 and 4 respectively.

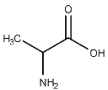
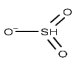
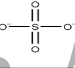
Among these, the discussed interaction between OH radicals and atomic oxygen is most prominent. Furthermore, the photo-dissociation of long-lived species (or their precursors, e.g. $\cdot NO_2$) occurring by increasing the treatment time could contribute to their decomposition in liquid both for N-containing species [61, 62], and for hydrogen peroxide [61, 63-66], mainly due to Ar excimers radiation ($\lambda_{MAX} = 126$ nm) as shown in **Fig. 4**. To support this hypothesis, the high amount of species from water photolysis in long distances with plasma-only, shown in **Fig. 7**. Even on long distances (12 mm) away from the effluent there is significant amount of VUV/UV detected (**Fig. 4**). Ar excimer intensity drops only $\sim 20\%$ from shortest (2 mm) to longest considered distance (12 mm). Consequently, it has to be noted that on longer treated distances (12 mm) UV radiation has leading role in plasma induced liquid chemistry. As previously discussed, the impact of radiation, as well as other reactive species in the gas phase (e.g. $\cdot O$ and $\cdot O_2$) is reduced by the presence of aerosol. This is a very important observation considering that VUV/UV radiation can have an impact on the density of long-living species in the liquid media. However, it has to be mentioned that (V)UV may also have a negative effect due to direct impact on biological samples, e.g. via lipid or protein photo-oxidation. Correspondingly, aerosol injection seems to be very effective method to control the amount of (V)UV radiation reaching the target as well as plasma induced chemistry in the liquid phase.

3.3 Cysteine oxidation is modulated by the aerosol

A significant oxidation of cysteine was observed with the thiol group as a main target (**Tab. 2**). Depending on the treatment, oxidation levels of cysteine vary: for short treatments, compounds with a lower oxidation number of sulfur dominate, such as cystine (2), cysteine sulfinic acid (3), cysteine *S*-sulfonate (6), and cysteine disulfoxides (7-9). These intermediates are not stable and are further oxidized by strong oxidizing conditions (e.g. long treatments, short distances) resulting in compounds with high oxidation states of sulfur, such as cysteine sulfonic acid (5) and sulfate (13), both end products of the cysteine oxidation pathway [29]. Some of the products indicate the presence of certain reactive species [67]: cystine for the presence of H₂O₂, cysteine-*S*-sulfonate for [•]OH radicals, cysteine sulfonic acid for gas-phase ROS ([•]O, ¹O₂), and cysteine sulfinic acid for both short-lived ROS ([•]O, ¹O₂) and water-derived [•]OH. Control measurement excluded effects of argon flow on cysteine. For the treatment of liquid targets without cysteine in the aerosol, a direct electron transfer was excluded since the effluent did not touch the liquid. The impact of heat was estimated by control tests performed by incubating cysteine for 1 min at 100 °C. A conversion of 17% cysteine to cystine was observed, and no other cysteine products were detected.

Table 2. Major cysteine derivatives induced by plasma treatment. Further details are described in previous publications [29, 60, 67].

No	Name	Formula	[M-H] ⁻ (m/z)	Reactive species*	Structure
1	Cysteine (RSH)	C ₃ H ₇ NO ₂ S	120.0119	none	
2	Cystine (RSSR)	C ₆ H ₁₂ N ₂ O ₄ S ₂	239.016	[•] OH, H ₂ O ₂	
3	Cysteine sulfinic acid (RSO ₂ H)	C ₃ H ₇ NO ₄ S	152.0017	[•] OH, [•] O, ¹ O ₂	
4	S-nitrosocysteine (RSNO)	C ₃ H ₅ N ₂ O ₃ S	149.0021	[•] NO, N ₂ O ₃ , [•] NO ₂ , ONOO [•]	
5	Cysteine sulfonic acid (RSO ₃ H)	C ₃ H ₇ NO ₅ S	167.9967	[•] O, ¹ O ₂ , O ₃	
6	Cysteine S-sulfonate (RSSO ₃ H)	C ₃ H ₇ NO ₅ S ₂	199.9687	[•] OH	
7	Cysteine disulfoxide I (RSO ₂ RS)	C ₆ H ₁₂ N ₂ O ₆ S ₂	271.0056	[•] OH, H ₂ O ₂	
8	Cysteine disulfoxide II (RSO ₂ RSSR)	C ₉ H ₁₆ N ₃ O ₈ S ₃	390.0100	[•] OH, H ₂ O ₂ , [•] O, ¹ O ₂ , O ₃	
9	Cysteine disulfoxone (RSO ₂ RSO ₂)	C ₆ H ₁₀ N ₂ O ₈ S ₂	301.9879	[•] OH, H ₂ O ₂	

10	Alanine (R)	$C_3H_7NO_2$	88.03985	Radicals, photolysis	
11	Sulfite (SO_3^-)	SO_3	79.95681	Radicals, photolysis, ROS	
12	Sulfate (SO_4^-)	SO_4	95.95173	Radicals, photolysis, ROS	

*Oxygen and nitrogen reactive species potentially generated by plasma reacting with cysteine to form the correspondent derivative

Species as O_2^- could not be detected by using this model, due to their low reactivity towards the thiol moiety in a physiological pH. While the anion sulfite SO_3^- is potentially involved in the formation pathway of the *S*-sulfonate [68-70], the sulfate ion SO_4^- is formed by over-oxidation of cysteine. Those two and the cysteine fragment alanine could be formed by plasma-derived (V)UV radiation alone via cleavage of the C-S bond and subsequent oxidation of the SH radical [71-73].

3.4.1 The plasma parameters determine the chemistry in the liquid bulk/the interface

The observed cysteine derivatives varied significantly with applied plasma power, treatment time and distance. To obtain quantitative data, the multiple reaction monitoring (MRM) was applied and key molecules in the cysteine oxidation pathway (cysteine – RSH (1), cystine – RSSR (2), cysteine *S*-sulfonate – $RSSO_3H$ (6), sulfinic acid – RSO_2H (3), and sulfonic acid - RSO_3H (5)) were absolutely quantified by HPLC-MS. The MRM technique is both sensitive and specific, relying on the detection of specific fragment ions.

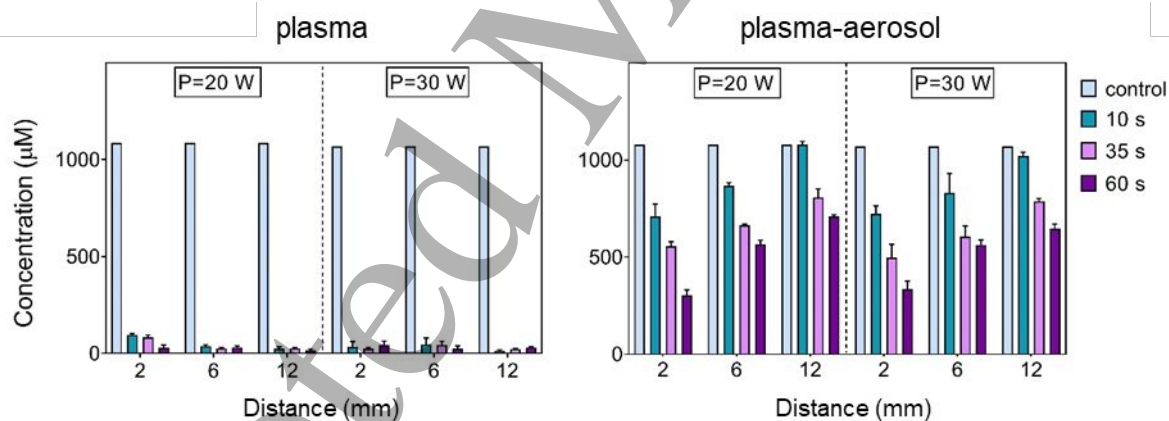


Figure 10. Absolute cysteine concentration after treatment of a cysteine solution by plasma with aerosol injection (setup 3, right) and without aerosol injection (setup 4, left). Power (20/30 W) and distance (2/6/12 mm) modulated. The injection of water into the plasma source massively changed reactive oxygen species output – the cysteine turnover is decreased markedly. See text. Mean of three independent experiments +SD.

Without aerosol injection, a strong, distance and treatment time independent cysteine oxidation was observed (**Fig. 10**). An almost complete oxidation of the available cysteine was observed and the residue was below 5%. In contrast, the presence of aerosol droplets reduced the oxidation efficacy markedly and the residual cysteine ranged between 100 % (20 W, 12 mm, 10 s) and 30 % (30 W, 2 mm, 60 s). Clearly, this indicates a “softer discharge” with a sharply decreased output of reactive oxygen species. The short-lived gas phase species O and 1O_2 are quenched by the presence of the water, and at the droplets surface water is cleaved forming $\cdot OH$ radicals that do

not survive the travel time (10 ms/2 mm). In contrast, when cysteine solutions are treated without aerosol injection, the local formation of $\cdot\text{OH}$ and $\cdot\text{H}$ by radiation and impact of argon excimers is promoted (see EPR data) and the additional impact of the short-lived gas phase species atomic O and $^1\text{O}_2$ leads to the observed strong cysteine oxidation (**Fig. 11**). Their presence is distance-dependent, the significant drop of the cysteine-S-sulfonate (6) at 12 mm distance proves the limited availability of atomic oxygen at the gas-liquid interface and subsequently $\cdot\text{OH}$ radicals in accordance with previous results [67]. The formation of highly oxidized cysteine derivatives was still substantial at 12 mm distances. This highlights the potential of the RF jet to produce reactive species surviving 6 mm and more travel distance such as singlet oxygen and (V)UV radiation (see **Fig. 4**). With these elements replacing the atomic oxygen, changes related to the distance were less significant than in the plasma-aerosol mode (**Fig. 12**). Cystine could be generated by recombination of thiyl radicals ($\text{RS}\cdot$) formed in reaction with $\cdot\text{OH}$ and $\cdot\text{H}$, or by reaction with H_2O_2 [74, 75]. Possibly, the synergistic effect of singlet oxygen and radiation is reflected in the sulfite and sulfate production. Indeed, radiation (vacuum UV) impact on cysteine molecules yielding to C-S breakage (bond energy 272 kJ mol⁻¹) [61]. The formed product could be further oxidized by oxygen species, e.g. singlet oxygen, to sulfate.

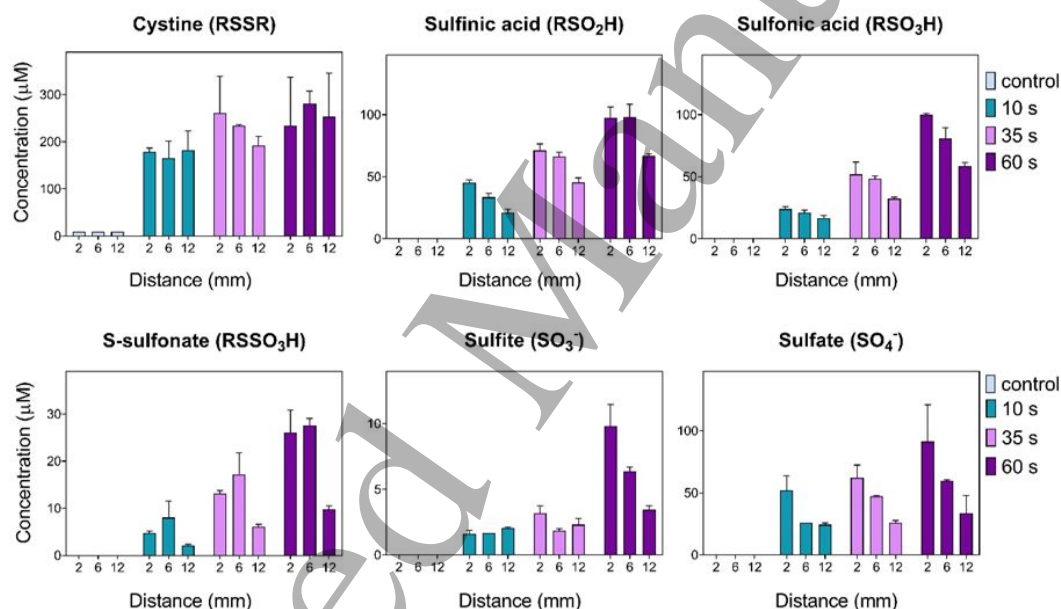


Figure 11. Absolute concentrations of cysteine derivatives after treatment by plasma without aerosol injection (setup 4, cysteine in target) at 30 W power. Time and distance were modulated. Mean of three independent experiments +SD. Cysteine oxidation products obtained with 20 W power are shown in **Fig. S3** and **S4**.

In presence of the aerosol the yield of the observed products changed, with some decreased (**Tab. 2**, compounds 2, 6, 12), others increased (**Tab. 2**, compound 11) or remained at similar level as under non-aerosol conditions (**Tab. 2**, compounds 3, 5). Obvious is a significant influence of the treatment distance, showing an inverted correlation with the product yield (e.g. cysteine sulfonic acid (5)). The pattern confirms the scavenging role of aerosol droplets in the effluent area for radiation and short-lived oxygen species. The resulting OH radicals are lost with distance leading to the observed loss in the yields of $\cdot\text{OH}$ -dependent derivatives (RSSR, RSSO₃H). Such, the formation of cysteine-S-sulfonate (**Tab. 2**, compound 6) occurred almost 10fold lower in the aerosol condition. In the presence of aerosol droplets, the formation of the stable derivative cysteine sulfonic acid (RSO₃H) increased

with treatment time and decreased significantly with the distance. In contrast, distance was of minor impact in the plasma-only mode (Fig. 11). Backed up by the EPR data (Fig. 7, 8) and the H₂O₂ deposition (Fig. 9), atomic oxygen and singlet oxygen represent the most likely candidates to explain this formation pattern. Only small amounts of H₂O₂ and OH radicals are deposited in the aerosol-mode at short distances. In contrast, TEMPD-adducts show the occurrence of singlet oxygen for both conditions and the presence of atomic oxygen at short distances/plasma-only conditions, along with the formation of cysteine sulfonic acid. The transport of ¹O₂ in the liquid droplets might occur for short distances, yielding to the high concentrations of sulfonic in this case. This assumption is not fully backed by the EPR data (Fig. 8), however, due to fact that the reaction probability with the respective spin probe/label does not allow absolute quantification the transport might not be reflected to a full extent. The ¹O₂ deposition further leads to the decay of intermediate products (RSO₂H, RSSO₃H) yielding to sulfonic acid (RSO₃H) for long treatments.

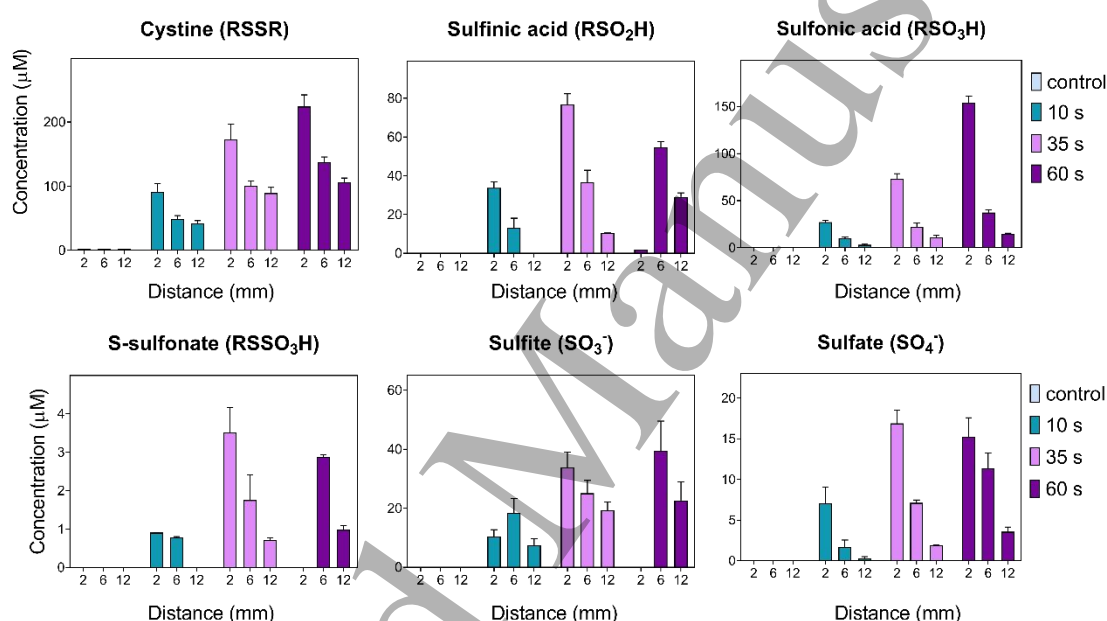


Figure 12. Absolute concentrations of cysteine derivatives after treatment by plasma with aerosol (setup 3, cysteine in target) at power 30 W. Time and distance were modulated. Mean of three independent experiments +SD. Cysteine oxidation products obtained with 20 W power are shown in Fig. S3 and S4.

An interesting and not fully resolved pattern is present for the two ions sulfite and sulfate that both represent fragmentation products of cysteine. They can be formed by different pathways, including impact of (V)UV radiation. The decrease of sulfate deposition in the presence of aerosol confirms role of the droplets as scavengers for radiation and reactive species.

3.4.2 Liquid chemistry induced in the aerosol droplets

The plasma-induced chemistry in the aerosol droplets was investigated to determine i) the type and fate during the transport in the effluent of the reactive species formed in the droplets, ii) the applicability of aerosol droplets as source of reactive species and carrier of drugs to be delivered on the biological target (Fig. 13). When introducing cysteine into the aerosol droplets, a significant extent of oxidation was observed. The extent depended on the traveling time – with longer distance between nozzle and target (either dry collection into plate or water), yielding

in stronger cysteine oxidation. For the 2 mm case when aerosol droplets remain 10 ms in the effluent zone, $37\% \pm 1.4$ and $39\% \pm 1.8$ of the available cysteine was oxidized. This impact was independent from collection time (10 s – 60 s), indicating that the majority of the reactions take place during the droplets transport to the target and not in the collection liquid/the droplet formed during collection. When quantifying the major cysteine derivatives for diverse distances and collection times (**Fig. 14**, **Fig. S5**), similar cysteine derivatives as for the treatment of a cysteine solution were observed. For longer distances, slightly higher amounts of the sulfinic acid (RSO_2H) and the S-sulfonate (RSSO_3H) were observed while the dominant product cysteine sulfonic acid remained unchanged. This sulfonic acid is a marker for short-lived gaseous ROS (e.g. O , $^1\text{O}_2$, [67]) showed a distance-insensitive behavior and accumulated during treatment time - its formation however only occurred during the passage through the active plasma zone emphasizing the interaction of the gas phase species with the surface of the droplets (Ar excimers and (V)UV photons, $\cdot\text{O}$, $^1\text{O}_2$). The formation of OH radicals seems to extend beyond the visible effluent zone (2 mm) for some time, as the increased formation of RSO_2H and RSSO_3H with distance suggest.

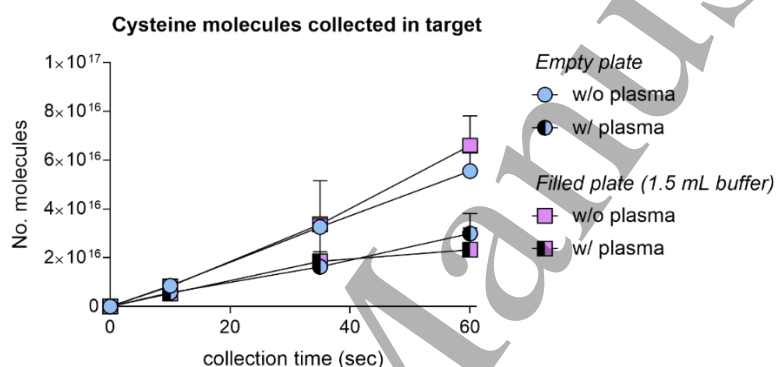


Figure 13. Cysteine turnover in aerosol droplets passing the plasma source with plasma off (full symbols) or plasma on (divided symbols) collected into empty wells (circles) and water filled wells (squares). Plasma power 30 W, 2 mm distance to target (setup 1 and 2). Cysteine oxidation occurs in the droplet during passage of the effluent only (10 ms).

These results confirmed the potential carrier role of droplets (e.g., for short-lived reactive oxygen species) in short distances, as well as their scavenging role towards radiation and short-lived reactive oxygen species in longer distances in favor of the production of water homolysis species, e.g., OH radicals (**Fig. 12**). Additionally, the presence of aerosols confirmed the possibility to deliver drugs on biological target, as shown by observing the trends of the cysteine delivery as model.

In this case, further investigations are needed to clarify potential modifications occurring on specific drugs, opening the possibilities to control the imported modifications in the use of plasma with aerosol injection for the delivery, and eventually activation of prodrugs in the effluent, before reaching the target.

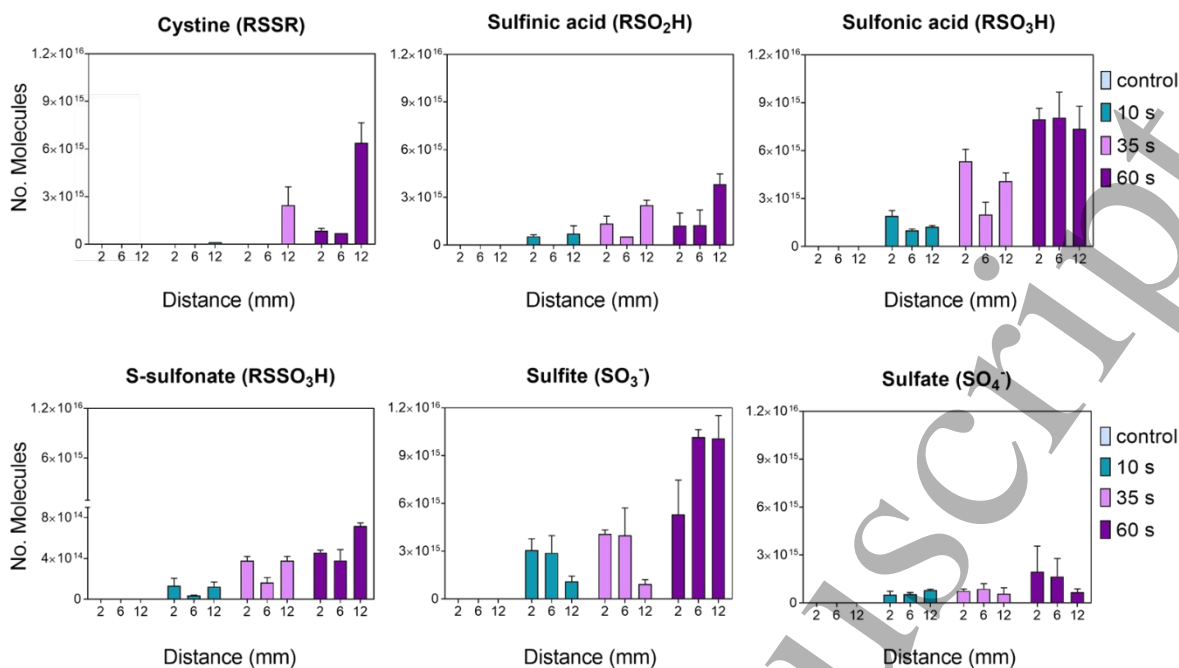


Figure 14. Major cysteine conversion products observed in cysteine-enriched aerosol droplets. Plasma power 30 W (setup 2, cysteine in aerosol), collected in water filled wells. The absolute number of molecules deposited are given. The limited impact of distance indicates that the majority of reactions occurs in the droplets. Further discussion see text.

3.4.3 Cysteine conversion pathways by RF jet derived species

In this work plasma interaction with liquid phase was investigated in 3 different model systems, namely, (i) plasma with cysteine in liquid target; (ii) plasma with aerosol and cysteine in liquid target; (iii) plasma interaction with cysteine-enriched aerosol injection into the effluent. To compare the effectiveness of different setups in terms of total cysteine oxidation and its conversion into derivatives, measured absolute concentration are hereby recalibrated in percentages % for each setup (**Fig. 15**). Additionally to the schematic of the cysteine oxidation, a complete overview for different treatment distances is summarized in **Tab. 3**.

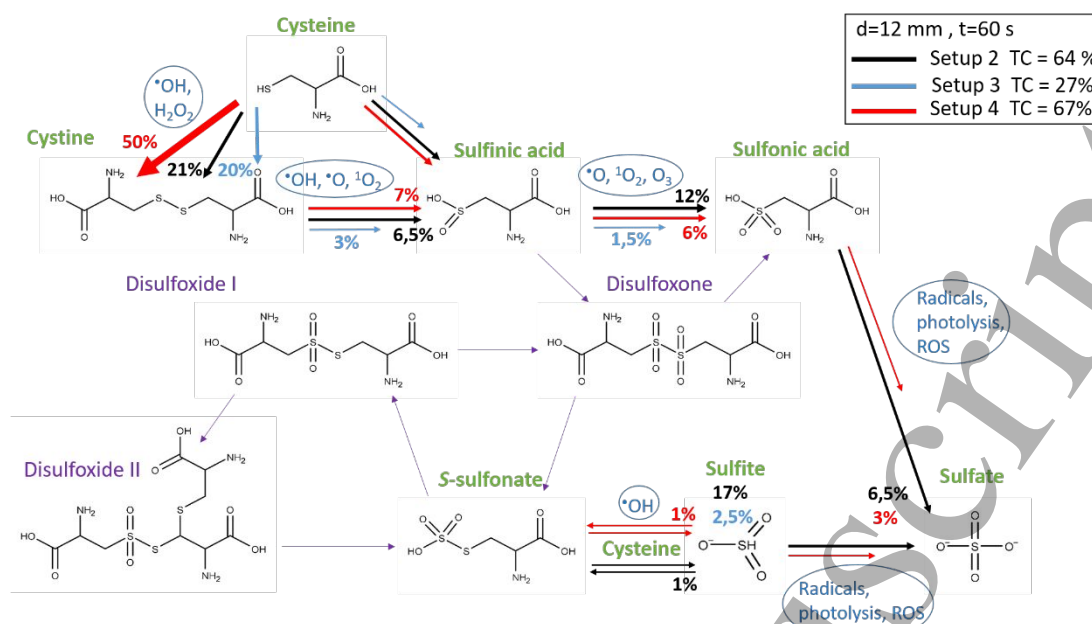


Figure 15. Cysteine oxidation pathway example and its total conversion for experimental parameters $P = 30$ W, $d = 12$ mm, $t = 60$ s. Generation of six major cysteine derivatives in Setup 2 (cysteine in aerosol, black), Setup 3 (plasma with aerosol-cysteine in target, blue) and Setup 4 (plasma-cysteine in target, red) is presented in percentage, for better comparison of processes. The quantified derivatives are labelled in green color.

As expected, the conversion of cysteine is highest for the direct plasma treatment of a cysteine-containing target liquid. In this case, the distance is of little importance and conversion is still massive at 12 mm. In contrast, when water droplets are injected into the effluent, the cysteine oxidation drops significantly even for 2 mm distance and further with increasing distance to the nozzle (**Tab. 3**). When the aerosol is enriched with cysteine, the observed product portfolio indicates that the majority of the reactions take place in the droplet during the passage of the visible effluent (10 ms/2 mm). The increase of the metastable cysteine products S-sulfonate and sulfenic acid with increasing distance show a residual formation of hydroxyl radicals beyond the effluent visible margins.

Table 3. Total cysteine conversion into 6 quantified derivatives during the treatment time of 60 s for treatment distances 2, 6 and 12 mm from effluent in Setups 2,3 and 4.

Setup	Treatment distance (mm)	Cysteine conversion (%)
Setup 2 Plasma treatment of cysteine in aerosol liquid	2	45
	6	50
	12	64
Setup 3 Plasma-aerosol treatment of cysteine in liquid target	2	60
	6	43
	12	27
Setup 4 Plasma treatment of cysteine in liquid target	2	78
	6	83
	12	67

It has to be emphasized that separate processes leading to cysteine oxidation were not disentangled here, but the overall effect on cysteine has been presented. Oxidation of cysteine can be assigned to the contribution of different

1
2
3 factors such as the direct effect of plasma on aerosol droplets passing through the plasma effluent, different
4 chemistry initiated by the discharge and VUV/UV radiation on cysteine in droplets and the target. Despite the
5 unknown contribution of listed oxidation factors in different treatment configurations and the exact number of
6 aerosol droplets interacting with effluent (Setup 2 and Setup 3), total effect on cysteine concentration has been
7 analyzed and a final concentration of the cysteine has been accordingly presented in Table 3.
8
9

10
11 It is important to point out that the possible control of the VUV radiation by decrease of the discharge power is
12 considered to be less effective in comparison to the aerosol injection. Indeed, decrease of the plasma power would
13 result in a lower production of ROS/RNS in the effluent region with still unavoidable emission of VUV below 180
14 nm. Correspondingly, an application of equivalent plasma treatment at lower plasma power, would require longer
15 treatment time while the target would be exposed to VUV emission. The aerosol injection in plasma effluent, on
16 the other hand modulates ROS/RNS chemistry, allowing to tailor the treatment dose and species deposition
17 desirable for biomedical application.
18
19
20

21 **4. SUMMARY AND CONCLUSION**

22
23 A RF plasma jet combined with an aerosol injection into the effluent has been developed for biomedical purposes.
24 The droplets allowed the modulation of the generated reactive species and the (V)UV emission intensity. Aerosol
25 droplets loaded with the model drug cysteine protected it from decomposition, suggesting the setup to be suitable
26 for the topical delivery of drugs, e.g. for promoting wound healing. Injection of the aerosol into the plasma effluent
27 influenced the plasma chemistry in terms of RONS and VUV/UV radiation production and their flux towards the
28 treated object, facilitating tailored application for medical purposes. The chemistry in the plasma-liquid
29 interface/boundary layer and the bulk liquid was analyzed using cysteine as a bait molecule, particularly focusing
30 on the role of aerosol droplets in the effluent. The deposition of OH, O₂⁻, and O, ¹O₂, and O₃ were measured via
31 EPR; and the long-lived species H₂O₂, NO₂⁻, and NO₃⁻ were quantified by colorimetric assays and ion
32 chromatography. Data analysis revealed that UV radiation (Ar excimers, atomic oxygen), followed by short-lived
33 reactive oxygen species (e.g. [•]O, ¹O₂), are the dominant active elements in the studied RF plasma jet. Acting
34 directly on the liquid target or on the aerosol droplets in plasma effluent, cysteine oxidation products and water
35 photolysis products ([•]OH, [•]H) were observed. A summary of the model and the observations made is presented in
36
37
38
39
40
41
42 **Figure 16.**
43
44
45
46
47
48
49
50
51
52
53
54
55
56
57
58
59
60

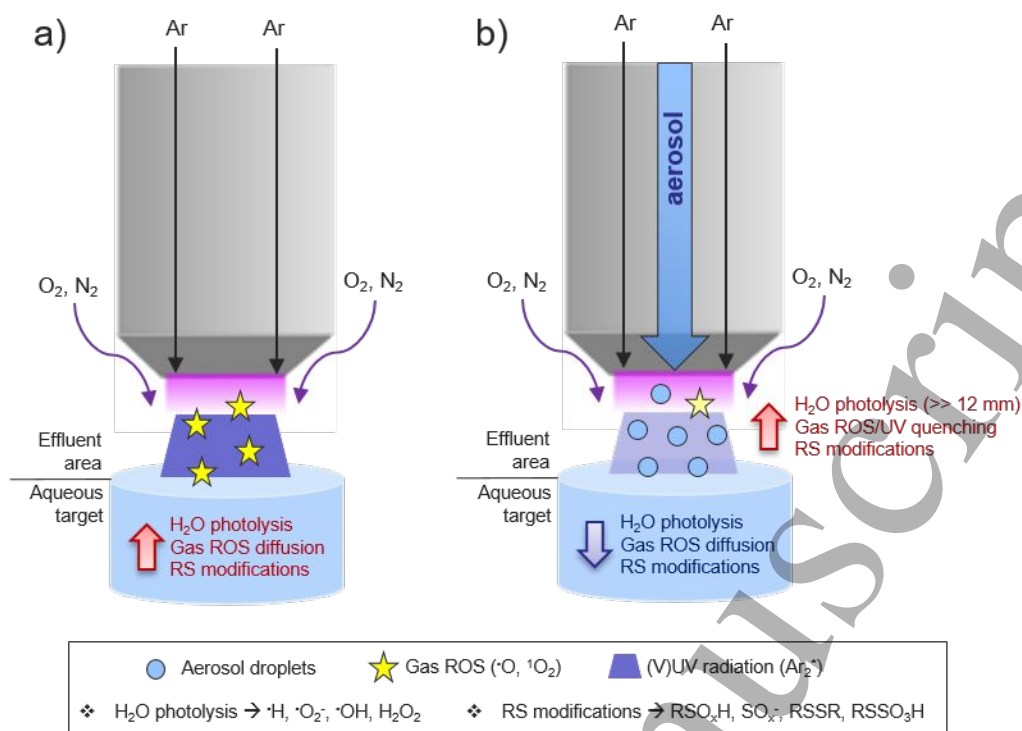


Figure 16. Overview of cold plasma effects without (a) and with (b) aerosol droplets in the effluent area.

By controlling distance, treatment time, and the presence of aerosol droplets the liquid phase chemistry can be adjusted in a wide range. Short-lived gaseous species (e.g. $\cdot\text{O}$, $^1\text{O}_2$) were detected predominantly for short distances and in parallel, distinct cysteine oxidation products were observed, confirming ROS potential biological impact. In the presence of aerosol droplets, the impact of these species was diminished significantly yet cysteine sulfonic acid, a marker for gas phase ROS at the gas-liquid interface, was still detected. Taking the EPR data into account it was concluded that singlet oxygen $^1\text{O}_2$ prevails for middle and long distances (6 - 12 mm) and in the presence of aerosol. The impact of (V)UV radiation on the liquid target was strong, leading to photo-dissociation of water molecules as well as cysteine and the formation of short-lived radicals (e.g. $\cdot\text{OH}$, $\cdot\text{H}$, SH), as confirmed by EPR and the detection of sulfite/sulfate by mass spectrometry. Again, the presence of aerosol droplets in the effluent lead to absorption of the (V)UV photons and related reactions in the target. Instead, water molecules in the droplets were attacked, forming e.g. OH radicals at the droplet's gas-liquid interface. The transport of species formed in or solvated by the droplets was found to be of minor importance. This hypothesis was confirmed by introducing cysteine solution directly in form of aerosol droplets and the observation of cysteine derivatives produced predominantly by OH radicals (cystine, sulfinic acid, cysteine-S-sulfonate). The impact of (V)UV radiation was observed by the formation of sulfite from cysteine-containing droplets.

In conclusion, the chemical potential of the investigated RF plasma jet coupled with aerosol allows to be modulated in a wide range, proposing its application for various biomedical purposes. The intense synergistic effects of radiation and short-lived gaseous species achieved by using the plasma-only mode could be relevant for cancer treatment. In contrast, softer conditions including aerosol droplets could limit the impact of radiation and other gaseous radical species, and be of interest in the wound care field where any possible side effect of VUV/UV has to be avoided.

ACKNOWLEDGEMENTS

The research work performed was supported by German Federal Ministry of Education and Research (grant number 03Z22DN12 to K.W.) and FWO/ARRS agencies project “Plasma-skin interactions: from wound treatment to topical introduction of molecules”, numbers G084917N and N3-0056, respectively.

CONFLICT OF INTEREST

The authors declare no conflict of interest.

REFERENCES

1. Laroussi, M., *Sterilization of contaminated matter with an atmospheric pressure plasma*. IEEE Transactions on Plasma Science, 1996. **24**(3): p. 1188-1191.
2. Laroussi, M., *Low temperature plasma-based sterilization: Overview and state-of-the-art*. Plasma Processes and Polymers, 2005. **2**(5): p. 391-400.
3. Weltmann, K.D., et al., *Atmospheric-pressure plasma sources: Prospective tools for plasma medicine*. Pure and Applied Chemistry, 2010. **82**(6): p. 1223-1237.
4. Weltmann, K.D. and T. von Woedtke, *Plasma medicine—current state of research and medical application*. Plasma Physics and Controlled Fusion, 2017. **59**(1): p. 014031.
5. Kong, M.G., et al., *Plasma medicine: an introductory review*. new Journal of Physics, 2009. **11**(11): p. 115012.
6. Fridman, A.A., et al., *The Plasma Treatment Unit: An Attempt to Standardize Cold Plasma Treatment for Defined Biological Effects*. Plasma Medicine, 2018. **8**(2): p. 195-201.
7. Stratmann, B., et al., *Effect of Cold Atmospheric Plasma Therapy vs Standard Therapy Placebo on Wound Healing in Patients With Diabetic Foot Ulcers: A Randomized Clinical Trial*. JAMA Netw Open, 2020. **3**(7): p. e2010411.
8. Bekeschus, S., et al., *Ex Vivo Exposure of Human Melanoma Tissue to Cold Physical Plasma Elicits Apoptosis and Modulates Inflammation*. Applied Sciences, 2020. **10**(6): p. 1971.
9. Schmidt, A., et al., *Nrf2 signaling and inflammation are key events in physical plasma-spurred wound healing*. Theranostics, 2019. **9**(4): p. 1066-1084.
10. Shome, D., et al., *The HIPPO Transducer YAP and Its Targets CTGF and Cyr61 Drive a Paracrine Signalling in Cold Atmospheric Plasma-Mediated Wound Healing*. Oxidative Medicine and Cellular Longevity, 2020. **2020**: p. 4910280-4910280.
11. Privat-Maldonado, A., et al., *ROS from Physical Plasmas: Redox Chemistry for Biomedical Therapy*. Oxidative medicine and cellular longevity, 2019. **2019**: p. 9062098.
12. Lin, A., et al., *Plasma Elicits Immunogenic Death In Melanoma Cells*. Clinical Plasma Medicine, 2018. **9**: p. 9.
13. Xu, X., *Dielectric barrier discharge—properties and applications*. Thin solid films, 2001. **390**(1-2): p. 237-242.
14. Brandenburg, R., *Dielectric barrier discharges: progress on plasma sources and on the understanding of regimes and single filaments*. Plasma Sources Science & Technology, 2017. **26**(5): p. 053001.
15. Reuter, S., T. Von Woedtke, and K.-D. Weltmann, *The kINPen—a review on physics and chemistry of the atmospheric pressure plasma jet and its applications*. Journal of Physics D: Applied Physics, 2018. **51**(23): p. 233001.
16. Bruggeman, P.J., et al., *Plasma–liquid interactions: a review and roadmap*. Plasma sources science and technology, 2016. **25**(5): p. 053002.

17. Sato, M., T. Ohgiyama, and J.S. Clements, *Formation of chemical species and their effects on microorganisms using a pulsed high-voltage discharge in water*. IEEE Transactions on Industry applications, 1996. **32**(1): p. 106-112.
18. Burlica, R., et al., *Bacteria inactivation using low power pulsed gliding arc discharges with water spray*. Plasma Processes and Polymers, 2010. **7**(8): p. 640-649.
19. Maguire, P., et al., *Controlled microdroplet transport in an atmospheric pressure microplasma*. Applied Physics Letters, 2015. **106**(22): p. 224101.
20. Oinuma, G., et al., *Controlled plasma–droplet interactions: A quantitative study of OH transfer in plasma–liquid interaction*. Plasma Sources Science and Technology, 2020. **29**(9): p. 095002.
21. Stancampiano, A., et al., *Plasma and aerosols: Challenges, opportunities and perspectives*. Applied Sciences, 2019. **9**(18): p. 3861.
22. Sremački, I., et al., *On diagnostics of annular-shape radio-frequency plasma jet operating in argon in atmospheric conditions*. Plasma Sources Science and Technology, 2020. **29**(3): p. 035027.
23. Sremački, I., et al. *Radio-frequency plasma in combination with aerosol injection for biomedical applications*. in *24th International Symposium on Plasma Chemistry*. 2019. International Plasma Chemistry Society (IPCS).
24. Hendawy, N., et al., *Continuous gas temperature measurement of cold plasma jets containing microdroplets, using a focussed spot IR sensor*. Plasma Sources Science and Technology, 2020. **29**(8): p. 085010.
25. von Woedtke, T., et al., *Plasma Medicine: A field of applied redox biology*. in vivo, 2019. **33**(4): p. 1011-1026.
26. Schieber, M. and N.S. Chandel, *ROS function in redox signaling and oxidative stress*. Current biology, 2014. **24**(10): p. R453-R462.
27. Weidinger, A. and A.V. Kozlov, *Biological activities of reactive oxygen and nitrogen species: oxidative stress versus signal transduction*. Biomolecules, 2015. **5**(2): p. 472-484.
28. Strollo, R., et al., *Antibodies to post-translationally modified insulin in type 1 diabetes*. Diabetologia, 2015. **58**(12): p. 2851-60.
29. Bruno, G., et al., *Cold physical plasma-induced oxidation of cysteine yields reactive sulfur species (RSS)*. Clinical Plasma Medicine, 2019. **14**: p. 100083.
30. Klinkhammer, C., et al., *Elucidation of Plasma-induced Chemical Modifications on Glutathione and Glutathione Disulphide*. Sci Rep, 2017. **7**(1): p. 13828.
31. Takai, E., et al., *Chemical modification of amino acids by atmospheric-pressure cold plasma in aqueous solution*. Journal of Physics D-Applied Physics, 2014. **47**(28): p. 285403.
32. Lackmann, J.W., et al., *Chemical fingerprints of cold physical plasmas - an experimental and computational study using cysteine as tracer compound*. Sci Rep, 2018. **8**(1): p. 7736.
33. Go, Y.M., J.D. Chandler, and D.P. Jones, *The cysteine proteome*. Free Radic Biol Med, 2015. **84**: p. 227-245.
34. Tresp, H., et al., *Quantitative detection of plasma-generated radicals in liquids by electron paramagnetic resonance spectroscopy*. Journal of Physics D: Applied Physics, 2013. **46**(43).
35. Jablonowski, H., et al., *Quantification of the ozone and singlet delta oxygen produced in gas and liquid phases by a non-thermal atmospheric plasma with relevance for medical treatment*. Sci Rep, 2018. **8**(1): p. 12195.
36. Jablonowski, H., et al., *Non-touching plasma-liquid interaction - where is aqueous nitric oxide generated?* Phys Chem Chem Phys, 2018. **20**(39): p. 25387-25398.
37. Verlackt, C.C.W., W. Van Boxem, and A. Bogaerts, *Transport and accumulation of plasma generated species in aqueous solution*. Phys Chem Chem Phys, 2018. **20**(10): p. 6845-6859.
38. Nikiforov, A.Y., et al., *Characterization of a planar 8 mm atmospheric pressure wide radiofrequency plasma source by spectroscopy techniques*. Plasma Physics and Controlled Fusion, 2015. **58**(1): p. 014013.
39. Jablonowski, H., et al., *Impact of plasma jet vacuum ultraviolet radiation on reactive oxygen species generation in bio-relevant liquids*. Physics of plasmas, 2015. **22**(12): p. 122008.

- 1
2
3 40. Bruggeman, P., et al., *Mass spectrometry study of positive and negative ions in a capacitively coupled atmospheric pressure RF excited glow discharge in He–water mixtures*. Journal of Physics D: Applied Physics, 2009. **43**(1): p. 012003.
- 4
5
6 41. Rosen, G.M., et al., *The role of tetrahydrobiopterin in the regulation of neuronal nitric-oxide synthase-generated superoxide*. J Biol Chem, 2002. **277**(43): p. 40275-80.
- 7
8 42. Tong, H., et al., *Hydroxyl radicals from secondary organic aerosol decomposition in water*. Atmospheric Chemistry and Physics, 2016. **16**(3): p. 1761-1771.
- 9
10 43. Lisovskaya, A.G., I.P. Edimecheva, and O.I. Shadyro, *A Novel Pathway of Photoinduced Decomposition of Sphingolipids*. Photochemistry and Photobiology, 2012. **88**(4): p. 899-903.
- 11
12 44. Zvereva, G.N., *Using vacuum ultraviolet radiation to obtain highly reactive radicals*. Journal of Optical Technology, 2012. **79**(8): p. 477-483.
- 13
14 45. Jablonowski, H., et al., *Plasma Jet (V) UV-Radiation Impact on Biologically Relevant Liquids and Cell Suspension*. Bulletin of the American Physical Society, 2014. **59**.
- 15
16 46. Attri, P., et al., *Generation mechanism of hydroxyl radical species and its lifetime prediction during the plasma-initiated ultraviolet (UV) photolysis*. Sci Rep, 2015. **5**: p. 9332.
- 17
18 47. Flyunt, R., et al., *Determination of •OH, O₂•⁻, and Hydroperoxide Yields in Ozone Reactions in Aqueous Solution†*. The Journal of Physical Chemistry B, 2003. **107**(30): p. 7242-7253.
- 19
20 48. Hoigne, J. and H. Bader, *Ozonation of water: kinetics of oxidation of ammonia by ozone and hydroxyl radicals*. Environmental Science & Technology, 1978. **12**(1): p. 79-84.
- 21
22 49. Hoigné, J., *The chemistry of ozone in water*, in *Process technologies for water treatment*. 1988, Springer. p. 121-141.
- 23
24 50. Gorbanev, Y., D. O'Connell, and V. Chechik, *Non-Thermal Plasma in Contact with Water: The Origin of Species*. Chemistry, 2016. **22**(10): p. 3496-3505.
- 25
26 51. Winter, J., et al., *Feed gas humidity: a vital parameter affecting a cold atmospheric-pressure plasma jet and plasma-treated human skin cells*. Journal of Physics D-Applied Physics, 2013. **46**(29).
- 27
28 52. Hideg, E., et al., *Pure forms of the singlet oxygen sensors TEMP and TEMPD do not inhibit Photosystem II*. Biochim Biophys Acta, 2011. **1807**(12): p. 1658-61.
- 29
30 53. Schmidt-Bleker, A., et al., *On the plasma chemistry of a cold atmospheric argon plasma jet with shielding gas device*. Plasma Sources Science & Technology, 2016. **25**(1): p. 015005.
- 31
32 54. Zhang, S.Q., et al., *Spatially resolved ozone densities and gas temperatures in a time modulated RF driven atmospheric pressure plasma jet: an analysis of the production and destruction mechanisms*. Journal of Physics D-Applied Physics, 2013. **46**(20): p. 205202.
- 33
34 55. Pekárek, S., *Non-Thermal Plasma Ozone Generation*. Acta Polytechnica, 2003. **43**: p. 5.
- 35
36 56. Reuter, S., T. von Woedtke, and K.D. Weltmann, *The kINPen-a review on physics and chemistry of the atmospheric pressure plasma jet and its applications*. Journal of Physics D-Applied Physics, 2018. **51**(23).
- 37
38 57. Van Gaens, W. and A. Bogaerts, *Kinetic modelling for an atmospheric pressure argon plasma jet in humid air*. Journal of Physics D: Applied Physics, 2013. **46**(27): p. 275201.
- 39
40 58. Quiller, R.G., et al., *Transient hydroxyl formation from water on oxygen-covered Au(111)*. J Chem Phys, 2008. **129**(6): p. 064702.
- 41
42 59. Lifshitz, C., *Reaction mechanism of mononegative atomic oxygen + water .fwdarw. hydroxide + hydroxyl at low incident ion energies*. The Journal of Physical Chemistry, 1982. **86**(18): p. 3634-3637.
- 43
44 60. Lackmann, J.-W., et al., *Nitrosylation vs. oxidation - How to modulate cold physical plasmas for biological applications*. PLoS One, 2019. **14**(5): p. e0216606.
- 45
46 61. Zoschke, K., H. Bornick, and E. Worch, *Vacuum-UV radiation at 185 nm in water treatment--a review*. Water Res, 2014. **52**: p. 131-45.
- 47
48 62. Goldstein, S. and J. Rabani, *Mechanism of Nitrite Formation by Nitrate Photolysis in Aqueous Solutions: The Role of Peroxynitrite, Nitrogen Dioxide, and Hydroxyl Radical*. Journal of the American Chemical Society, 2007. **129**(34): p. 10597-10601.
- 49
50 63. Gölzenleuchter, H., et al., *Photodissociation of hydrogen peroxide at 157 nm: rotational distribution of nascent OH(2Σ⁺, v', N')*. Chemical Physics, 1984. **89**(1): p. 93-102.
- 51
52
53
54
55
56
57
58
59
60

- 1
2
3 64. Nakamura, K., et al., *Hydroxyl radicals generated by hydrogen peroxide photolysis recondition biofilm-contaminated titanium surfaces for subsequent osteoblastic cell proliferation*. *Sci Rep*, 2019. **9**(1): p. 4688.
- 4
5
6 65. Ikai, H., et al., *Photolysis of hydrogen peroxide, an effective disinfection system via hydroxyl radical formation*. *Antimicrob Agents Chemother*, 2010. **54**(12): p. 5086-91.
- 7
8 66. France, J.L., M.D. King, and J. Lee-Taylor, *Hydroxyl (OH) radical production rates in snowpacks from photolysis of hydrogen peroxide (H₂O₂) and nitrate (NO₃⁻)*. *Atmospheric Environment*, 2007. **41**(26): p. 5502-5509.
- 9
10
11 67. Wende, K., et al., *On a heavy path – determining cold plasma-derived short-lived species chemistry using isotopic labelling*. *RSC Advances*, 2020. **10**(20): p. 11598-11607.
- 12
13 68. Bailey, J.L. and R.D. Cole, *Studies on the Reaction of Sulfite with Proteins*. *Journal of Biological Chemistry*, 1959. **234**(7): p. 1733-1739.
- 14
15 69. Gunnison, A.F. and E.D. Palmes, *Species variability in plasma S-sulfonate levels during and following sulfite administration*. *Chemico-Biological Interactions*, 1978. **21**(2-3): p. 315-329.
- 16
17 70. Gunnison, A.F. and A.W. Benton, *Sulfur dioxide: Sulfite. Interaction with mammalian serum and plasma*. *Arch Environ Health*, 1971. **22**(3): p. 381-8.
- 18
19 71. Darwent, B.d., *Bond dissociation energies in simple molecules*. NSRDS-NBS31. 1970, [Washington]: U.S. National Bureau of Standards; for sale by the Supt. of Docs., U.S. Govt. Print. Off. iv, 48 p.
- 20
21 72. Mackle, H., *The thermochemistry of sulphur-containing molecules and radicals—II*. *Tetrahedron*, 1963. **19**(7): p. 1159-1170.
- 22
23 73. Jablonowski, H., et al., *Impact of plasma jet vacuum ultraviolet radiation on reactive oxygen species generation in bio-relevant liquids*. *Physics of Plasmas*, 2015. **22**(12): p. 122008.
- 24
25 74. Kalyanaraman, B., *Thiyl radicals in biological systems: significant or trivial?* *Biochem Soc Symp*, 1995. **61**: p. 55-63.
- 26
27 75. Sevilla, M.D., D. Becker, and M. Yan, *The formation and structure of the sulfoxyl radicals RSO(.), RSOO(.), RSO₂(.), and RSO₂OO(.) from the reaction of cysteine, glutathione and penicillamine thiyl radicals with molecular oxygen*. *Int J Radiat Biol*, 1990. **57**(1): p. 65-81.
- 28
29
30
31
32
33
34
35
36
37
38
39
40
41
42
43
44
45
46
47
48
49
50
51
52
53
54
55
56
57
58
59
60